Journal of Photochemistry & Photobiology, A: Chemistry 439 (2023) 114583

Contents lists available at ScienceDirect

Journal of Photochemistry & Photobiology, A: Chemistry

journal homepage: www.elsevier.com/locate/jphotochem

Tuning the competition between photoisomerization and photothermy in biomimetic cyclocurcumin analogues

Jérémy Pecourneau [a], Raúl Losantos [b,c], Axel Gansmuller [d], Stéphane Parant [a], Yann Bernhard [a], Maxime Mourer [a], Antonio Monari [b,*], Andreea Pasc [a,*]

[a] Université de Lorraine, CNRS, L2CM UMR 7053, F-54000 Nancy, France
[b] Université Paris Cité and CNRS, ITODYS, F-75006 Paris, France
[c] Universidad de La Rioja, Department of Chemistry, CISQ, 26006 Logroño, Spain
[d] Université de Lorraine, CNRS, CRM2 UMR 7036, F-54000 Nancy, France

ARTICLE INFO

Keywords:
Pyrone
Cyclocurcumine
Fluorescence
Photoswitch
Photothermal conversion

ABSTRACT

We report the synthesis and photophysical characterization of biomimetic D-A-D' cyclocurcumin derivatives, which can potentially be used in light activated chemotherapy. Particularly we highlight that both the donor (D) and acceptor (A) groups significantly influence the photophysical response of the chromophore inducing strong bathochromic shift with D/A strength increase and notable fluorescence quantum yield enhancement with donor strength increase. More important, the nature of the acceptor group (oxo or malonitrile) dramatically modifies the outcome in non-radiative deactivation channels. Indeed, while compounds functionalized with an oxo-moiety undergo ethylenic $E \rightarrow Z$ photoisomerization, the one bearing a malonitrile group leads exclusively to other non-adiabatic internal conversion channels which much favor photothermal conversion as no isomerization of the ethylenic double bond was observed. The tuning of the photophysical properties and the alteration of isomerization vs photothermal conversion is rationalized through the analysis of the potential energy surfaces along the most relevant degrees of freedom and shows a competitive pathway over malonitrile rotation. Our results offer novel perspective in oxygen-independent light activated chemotherapy and in the control of photochemical processes in biomimetic chromophores.

1. Introduction

The development of more selective and efficient antitumor therapies, which maintain a high cytotoxicity against cancer cells while minimizing generally toxicity and side effects is still of outmost importance. This is particularly true when addressing highly aggressive cancers developing strong resistance against conventional chemotherapy, like in the case of triple negative breast cancer [1] or pancreatic adenocarcinoma [2].

In this context, a promising alternative which has emerged in the last decades is based on the combined use of antitumoral drugs which are activated by the use of visible or infrared light, a strategy which is known under the general name of light activated chemotherapy (LAC). [3–4] The advantages of LAC over general chemotherapy or radiotherapy are the higher selectivity due to the localized irradiation that activates the drug and triggers the cellular response. Undoubtedly, the most widespread application of LAC has been achieved through the PhotoDynamic Therapy (PDT) framework, [5–6] in which the active drug, *i.e.* the sensitizer, populates its triplet state manifold and further induces energy transfer to the ground state molecular oxygen $^3O_2$ to produce the highly reactive singlet oxygen $^1O_2$. Nowadays PDT is efficiently applied clinically to treat different cancers, especially involving either throat and neck or the urogenital system due to the easier application of light sources. [7–9] PDT is also used as a complement in surgical tumor excision [10] to ensure a complete removal of the lesioned cells while minimizing the damages to the nearby tissues, or as a therapy for more benign conditions, including skin infections or psoriasis. [11] Despite its success, PDT suffers from some important drawbacks. Indeed, absorption in the far red or infrared region of the electromagnetic spectrum is necessary to reach a reasonable penetration of light into the body tissue, without causing accessory damages. The use of two photon absorbing dyes or triplet up conversion agents, as well as plasmonic nanoparticles [12,13] have been proposed to palliate this issue. Furthermore, the low solubility and bioavailability of PDT drugs

* Corresponding authors.
E-mail addresses: antonio.monari@u-paris.fr (A. Monari), andreea.pasc@univ-lorraine.fr (A. Pasc).

https://doi.org/10.1016/j.jphotochem.2023.114583
Received 24 November 2022; Received in revised form 20 January 2023; Accepted 23 January 2023
Available online 25 January 2023
1010-6030/© 2023 Elsevier B.V. All rights reserved.

might require encapsulation into supramolecular aggregates. [14–16] Labeling the carrier with specific antibodies should further enhance the selectivity and minimize side effects. [17] Finally, the action mechanism of PDT relies on the activation of oxygen, and hence its efficacy can be limited in the case of solid tumors developing hypoxia. [18–20] Furthermore, the rather unspecific reactivity of $^1O_2$ may in some case lead to cell death by necrosis, a pro-inflammatory event, which not only limits the quality of life of the patients due to intense pain but may also lead to serious complications. [21].

Other forms of LAC involving the use of organometallic complexes to achieve the photorelease of reactive oxygen (ROS) or nitrogen (RNS) species have been recently proposed but, although promising, are less generalized. [22–24] A complementary approach to PDT is Photo-Thermal Therapy (PTT), [25–27] in which the photochemistry of the photoactivable drug is dominated by non-radiative relaxation channels, which ultimately ends up in the excitation of the vibrational degrees of freedom and hence in a temperature increase. The local effect of PTT may be sufficiently high to lead to cell death under illumination. Usually, PTT agents involves either metallic nanoparticles or aggregating chromophores featuring moieties with floppy and large amplitude vibrational degrees of freedom, [28–31] thus offering effective non-radiative decay channels.

The use of molecular photoswitches as possible agents in LAC approaches has been recently reported by different groups. [32] In particular our groups have considered biomimetic analogues of cyclocurcumin (CC), a natural compound present in turmeric extracts together with the more common curcumin. [33–37] Interestingly, both curcumin and CC may present antiparasitic and antibiotic activity and have been proposed in a PDT framework for food decontamination. [38–39] Both the natural CC and our derived chromophore possess an isomerizable double bond which can undergo $E \rightarrow Z$ isomerization. We have shown that, differently from the natural compound, our biomimetic analogous isomerizes under the effect of visible light independently of the solvent environment, and may interact with model lipid membranes. [33] Furthermore, we have also confirmed, from an experimental and theoretical standpoint, that the isomerization is perturbing the membrane structural properties without its complete disruption. This property could then possibly trigger the apoptotic signal pathways, offering an original approach to LAC. [37].

In the present contribution we pursue the study of biomimetic analogs of cyclocurcumin (CC) involving different donor (hydroxy, ether, amine) and acceptor (oxo, malonitrile) groups, especially characterizing their optical, photophysical, and photochemical properties. Interestingly, we show that the modulation of the acceptor group leads to a very different non-radiative relaxation of the excited states. Indeed, while the presence of the oxo group favors $E \rightarrow Z$ isomerization, its replacement by malonitrile block the isomerization and therefore much largely activates vibrational relaxation, leading to increased photothermal conversion. The reasons behind switch in the non-radiative decay balance of the two compounds is also rationalized by the study of the potential energy surface (PES) landscape through molecular modeling and simulation at multiconfigurational wave-function level. In addition, when the donor group is strengthened (from ether to amine), both photothermal conversion efficiency and fluorescence build up, opening ways for theranostic approaches.

Our results not only show the fine modulation of the photophysical properties depending on different donor and acceptor groups, but also highlight the versatility of the present CC chromophores and their possible synergistic utilization in LAC applications and especially in PTT, after appropriate encapsulation to increase their colloidal stability in aqueous media and full pharmaco- and toxicological characterization (in dark conditions and under illumination).

2. Results and discussion

2.1. Synthesis of biomimetic CC analogous

Our oxo-containing chromophores were obtained from compound **1**, which was synthesized according to the previously reported procedures, and different vanillin **2a-d** substrates. Intermediate compounds **3a-d** have been produced by aldolization/crotonization in the presence of freshly prepared sodium ethanolate in moderate to good yields (from 38 to 59 %). The deprotection of the aryl-γ-pyrone units in acidic medium leads to the first family of oxo-derivatives, compounds **4a-d**, in excellent yields (greater than80 %) (Scheme 1). [33–34].

Those later were also used as building blocks to synthesize the second family of compounds bearing a malonitrile acceptor group (Scheme 2). The compounds **5a-d** were obtained by Knoevenagel condensation in acetic anhydride medium with excellent yields (greater than80 %) except for the derivative bearing the dimethylamine moiety (**5d**, 54 %). Their deprotection under mild basic conditions provided the malonitrile family of compounds **6a-d** (Scheme 2).

All the final products and intermediates were characterized by $^1H/^{13}C$ NMR and high-resolution mass spectroscopy (HRMS), confirming their molecular structures.

2.2. Photophysical properties

The steady state photophysical properties analysis of compounds **4a-d** and **6a-d** were performed in protic and aprotic solvents covering a broad polarity range going from toluene to methanol. Despite its relevance for biological applications, water was excluded due to the limited solubility of the compounds. Indeed, solubility in water remained too low for accurate spectroscopic analysis even after the addition of about 1 % of DMSO and the ultrasonication of the solutions.

Steady-state absorption spectra are shown in Fig. 1 and correspond to the thermodynamically favored *E*-isomer, estimated from ^1H NMR analysis to be formed at 92 % in the as-synthesized compound.

Regardless the solvent, the absorption spectra of the oxo-photoswitches bearing a hydroxy or alkoxy donor group (compounds **4a-c**) show three broad peaks centered around 290, 320, and 370 nm, similar to those of natural CC. [40–41] A bathochromic shift is observed for the amino compound **4d** with bands centered around 320 and 390 nm. This shift can be explained by the more pronounced donor capability of amine with respect to hydroxy or alkoxy moieties. Due to the acceptor modification and the corresponding increase of π conjugation, malonitrile derivatives **6a-d** present absorption bands at higher wavelength in all the solvents, peaking around 290 and 410–440 nm (Fig. 1 and S1, Table 1 and S1). In addition, a bathochromic shift in both absorption and emission is observed when increasing the solvent polarity.

The molar extinction coefficients at the band of maximum intensity (360–370 nm and 410–430 nm for compounds **4a-d** and **6a-d**, respectively) are depending on the solvent polarity as well as on the donor or acceptor peripheral groups (Tables 1 and S1). Indeed, the maximum absorbance is obtained for chloroform (35.3 and 55.1•10^3 M^{-1}•cm^{-1} for **4c** and **6a**, respectively) while the minimum corresponds to ethanol (27.5 and 52.2•10^3 M^{-1}•cm^{-1} for **4c** and **6a**, respectively). Molecular modeling of the absorption spectra, reported in SI (Fig. S2), reproduces well the global features of the experimental bands when considering dynamic and vibrational effects through a Wigner sampling of the Franck-Condon region.

The fluorescence spectra were obtained under excitation at the maximum absorbance and are given in Fig. 1 and S1 and Tables 1 and S1. The maximum of the fluorescence band is red-shifted when increasing the solvent polarity and Lippert-Mataga diagrams confirm a higher dipole moment for the excited than for the ground state (Fig. S3). [33] In all solvents, the fluorescence quantum yields of the compounds bearing hydroxy or alkoxy moieties (**4a-c** and **6a-c**) are low and do not

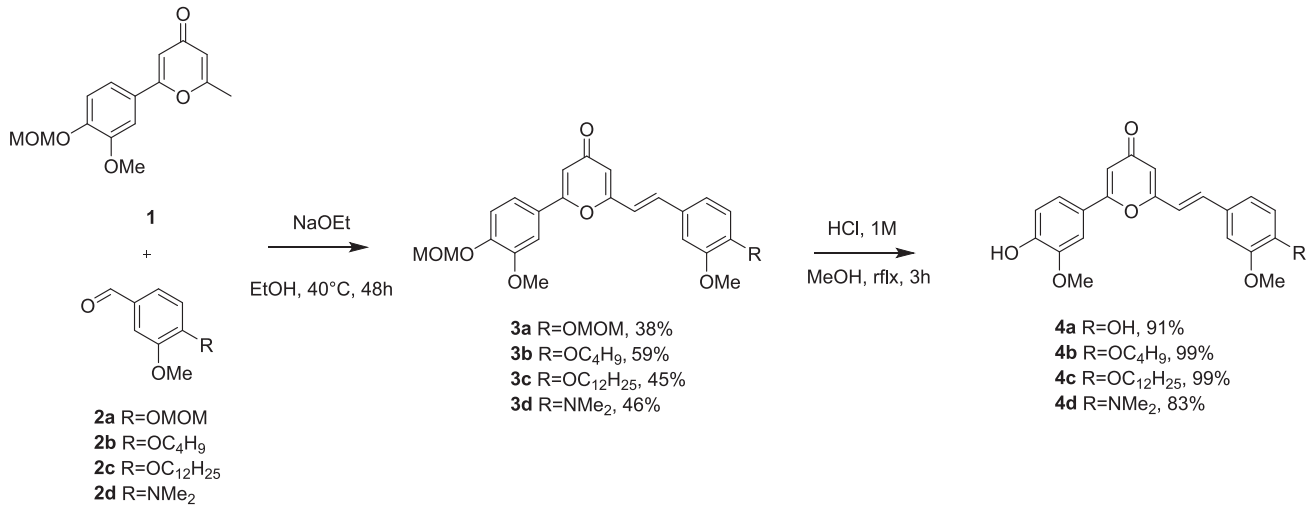

Scheme 1. Synthetic pathway leading to the biomimetic oxo-photoswitches, biomimetic analogs of CC.

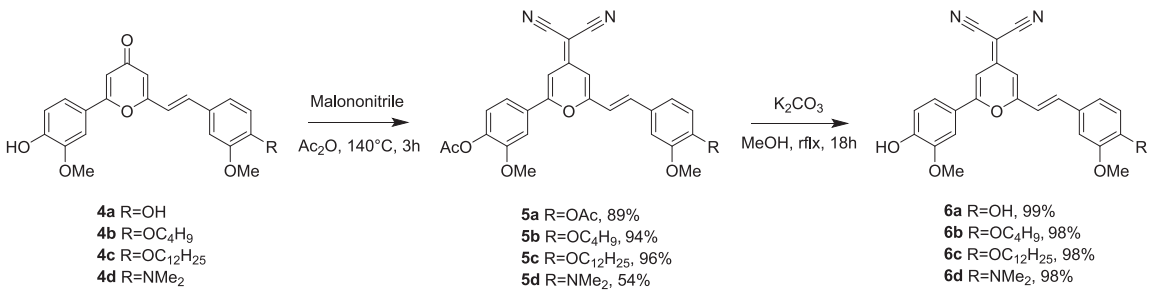

Scheme 2. Synthetic pathway leading to malo-compounds **6a-d** starting from keto-compounds **4a-d.**

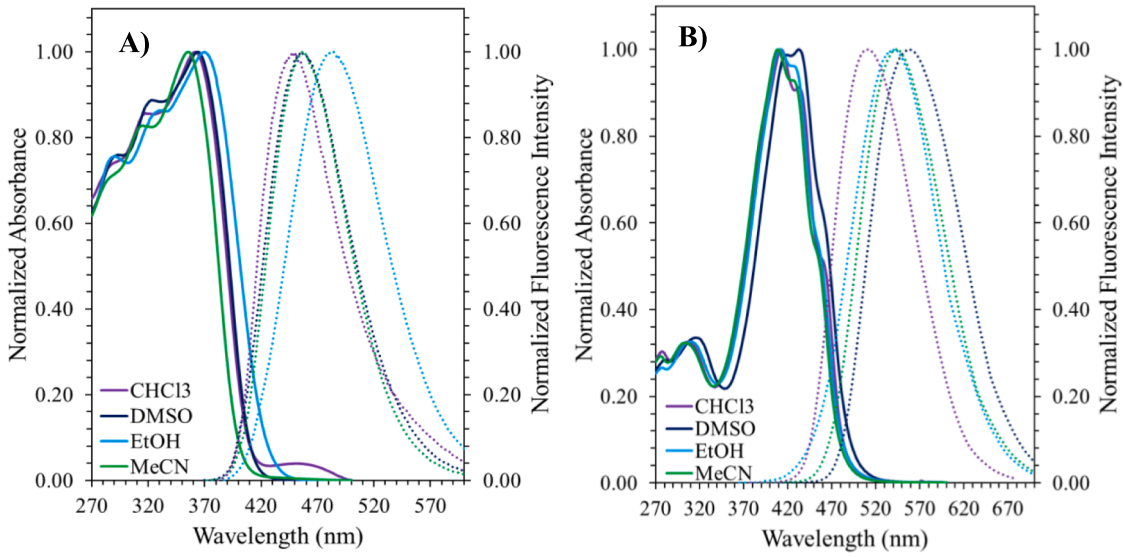

Fig. 1. Normalized absorption (full line) and emission (dashed line) spectra of compounds **4c** (A) and **6c** (B) in chloroform, acetonitrile, DMSO, and ethanol. Emission is obtained upon excitation at λ^{max}.

exceed 3 % ($\Phi_F = 0.03$). In contrast, compounds **4d** and **6d** (amine donor) have quantum yields of about 11 % (Table 1 and S1). The low fluorescence quantum yields could be explained by other competitive non-radiative deexcitation pathways, such as photoisomerization or vibrational relaxation.

As shown in Fig. 2 the natural transition orbitals (NTOs) [42] obtained for the lowest laying excited states show a different behavior depending on the presence of the oxo or malonitrile substituent. Indeed, compound **4d** shows a low energy absorption which is dominated by two main diabatic states, namely n-π* and π-π* transition. This pattern is absolutely coherent with the behavior of other similar CC derivatives namely **4a** and **4b** and may also explain the slight solvent dependency

Table 1
Optical properties of **4a-d** and **6a-d.** The maxima absorption, λ_{abs}, and emission, λ_{em}, are given in nm and the molar extinction coefficient, ε, in $M^{-1}\bullet cm^{-1}$. Φ_F stands for the fluorescence quantum yield.

Chromophore	Absorption / Emission	Solvent			
		Chloroform	*Acetonitrile*	*DMSO*	*Ethanol*
4a	λ_{abs} (ε•10^3)	358 (27)	354 (31.7)	367 (27.9)	374 (27.2)
	λ_{em} (Φ_F)	441 (0.02)	455 (0.01)	472 (0.02)	501 (0.02)
4b	λ_{abs} (ε•10^3)	363 (34.6)	356 (31.2)	364 (31)	368 (29.5)
	λ_{em} (Φ_F)	451 (0.02)	457 (0.01)	459 (0.01)	485 (0.01)
4c	λ_{abs} (ε•10^3)	362 (35.3)	356 (32.2)	364 (31)	370 (27.5)
	λ_{em} (Φ_F)	448 (0.02)	457 (0.01)	456 (0.01)	483 (0.01)
4d	λ_{abs} (ε•10^3)	388 (29)	384 (29)	394 (28.3)	391 (25.9)
	λ_{em} (Φ_F)	534 (0.09)	555 (0.08)	553 (0.11)	584 (0.09)
6a	λ_{abs} (ε•10^3)	411 (55.1)	407 (53.4)	430 (54.9)	413 (52.2)
	λ_{em} (Φ_F)	548 (0.01)	521 (0.02)	575 (0.01)	557 (0.01)
6b	λ_{abs} (ε•10^3)	413 (51.1)	408 (49.9)	417 (51.3)	410 (50.7)
	λ_{em} (Φ_F)	519 (0.01)	548 (0.03)	560 (0.02)	546 (0.01)
6c	λ_{abs} (ε•10^3)	412 (47.3)	408 (46.1)	416 (46.4)	411 (47)
	λ_{em} (Φ_F)	512 (0.01)	543 (0.02)	556 (0.01)	540 (0.01)
6d	λ_{abs} (ε•10^3)	424 (58.6)	420 (57.7)	432 (58.9)	423 (57.2)
	λ_{em} (Φ_F)	617 (0.11)	677 (0.04)	684 (0.08)	661 (0.06)

observed for absorption and emission. [35] Furthermore, as it will be detailed later, the electronic density reorganization involving the population of antibonding orbitals localized on the styryl double bond, pointing to a possible photoisomerization.

The presence of malonitrile moiety in **6d** significantly modifies the excited state landscape. The lowest excited state can now be described as a π-π* involving the malonitrile and the styryl double bond, while the second excited state accumulates electronic density on the phenyl ring directly bound to the pyran (D) while S_3 appears slightly more localized on the malonitrile substituent. Even from this first qualitative analysis a different photochemical behavior can, therefore, be surmised, since the photoisomerization pathway appears less favorable than in the original CC analogous.

2.3. Photoisomerization properties of the *4a-d* series

The photochemistry of the series **4a-d** can be assigned to a reversible photoinduced *E/Z* isomerization process, in which the direct switch corresponds to the conversion of the thermodynamically favored *E*-isomer into *Z*-isomer under illumination at 375 nm. The reverse process (back switch), *i.e.* $Z \rightarrow E$ photoisomerization, occurs by irradiation at 300 nm or thermally in the dark. The photoisomerization process was confirmed by in-situ irradiation ^{1}H NMR and UV–vis spectroscopy. ^{1}H NMR experiments were performed in four solvents ($CDCl_3$, DMSO-d_6, Acetonitrile-d_3, and Ethanol-d_6) at both ground state (GS) and photostationary state (PSS). E/Z ratio could be quantified by monitoring ^{1}H signal of styryl and methoxy groups, the latest giving the most accurate results due to their ideal resolution and lack of overlapping (Figures S4 and S5). As an example, the protons of the two $-OCH_3$ groups were found in $CDCl_3$ at 3.99 and 3.94 ppm for *E*-isomer and 3.70 and 3.65 ppm for *Z*-isomer, respectively.

The time-evolution of the absorption spectrum for all the compounds under irradiation at 375 nm and 300 nm was also analyzed in the same solvents. UV–vis spectra of the direct and reverse switch are given in Fig. 3 for **4c,d** and in figures S6 and S7 for **4a,b**. As expected, under irradiation at 375 nm one can observe the decrease of the bands corresponding to the π-π* transition for the *E*-isomer comprised between 370 nm and 385 nm depending on the chromophore. On the other hand, the back switch from PSS to GS is confirmed by the increase of the same band under irradiation at 300 nm.

As shown in Table 2, at the GS, the *E/Z* ratio is independent on the nature of the solvent (more than 92 % *E*-isomer for all compounds). Nevertheless, the efficiency of the photoisomerization varies with both the solvent and donor groups. For a given solvent, the conversion rates for compound **4c** are close to those previously determined for compounds **4a** and **4b** (about 80 %, 80 %, and 50 % in $CDCl_3$, Acetonitrile-d_3, DMSO-d_6, respectively). A significant decrease in photoisomerization efficiency was observed in ethanol-d_6 with increased carbon chain length and thus hydrophobicity (around 50 % for **4c** vs 65 % for **4b**). This could be due to the limited solubilization and possible self-aggregation. Compound **4d** showed a conversion rate evaluated at more than 70 % in $CDCl_3$ while it is of only 37 % in DMSO-d_6 and 15 % in Ethanol-d_6.

The back-switch at 300 nm irradiation did not allow to fully recover the initial *E*-isomer (Table 2). Indeed, only between 50 % and 85 % of **4c** was recovered. For **4d**, 85 % and 83 % of the *E*-isomer is obtained in

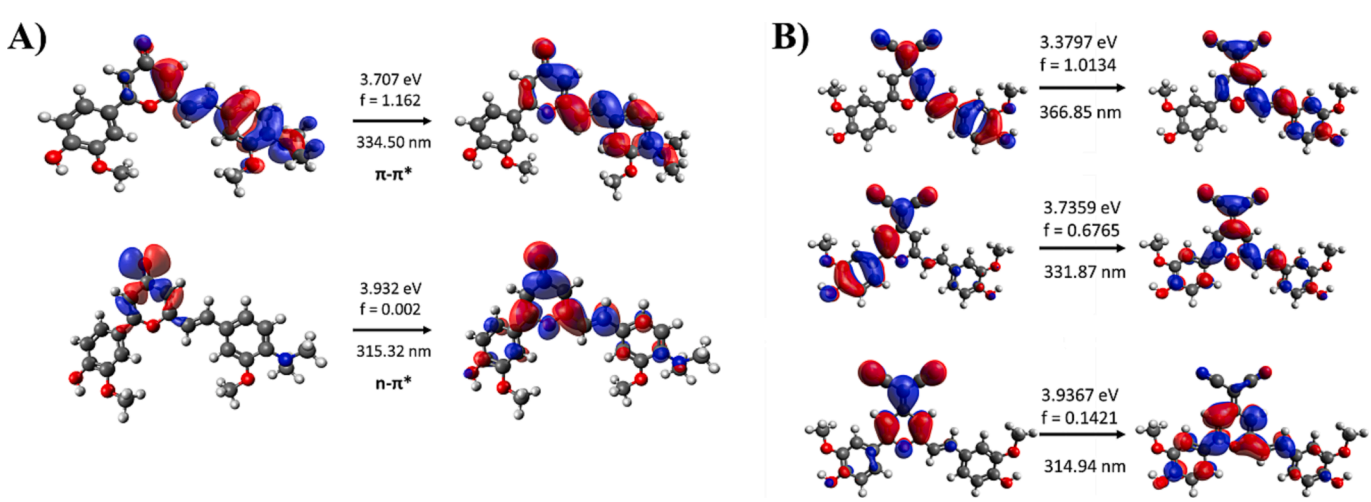

Fig. 2. NTOs describing the lowest electronically excited states for **4d** (A) and **6a** (B).

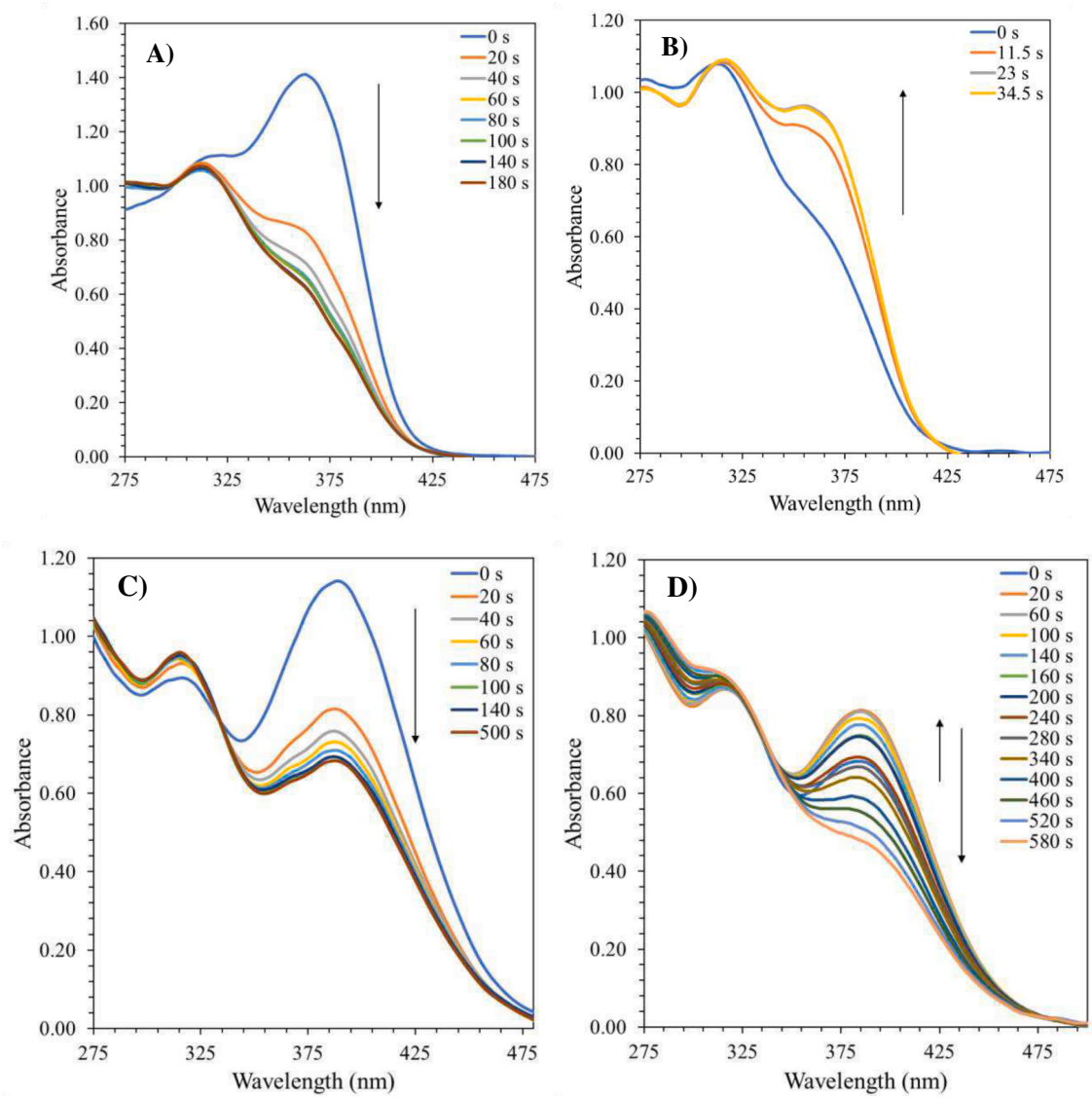

Fig. 3. Spectral evolution of the photoisomerization of compounds **4c** from the GS under irradiation at 375 nm in chloroform (A) and back switch after irradiation of the PPS at 300 nm (B). Spectral evolution of **4d** for the direct switch (C) and back switch (D) with the same condition as for **4c**.

acetonitrile-d_3 and DMSO-d_6, respectively. Interestingly, the back-switch is more effective in ethanol as a total conversion of **4d** to the initial *E/Z* ratio of 95/5 was observed. All those results agree well with the literature. [33–34] Moreover, a full degradation of **4d** in $CHCl_3$ was noticed which can be explained as an effect of the degradation of the solvent at 300 nm irradiation, leading to the formation of HCl. Indeed, mass spectrometry analysis of the compound obtained after irradiation coupled with UV analysis revealed the addition of HCl to the ethylenic double bond.

Except for this issue, the photoisomerization was perfectly reversible for all the compounds and in all solvents, over at least 10 cycles under successive irradiation at 375 nm (1.5 W, 10 s) and 300 nm (350 mW, 30 s). Furthermore, the isomerization occurred within several minutes despite the moderate power of the LEDs used as the illumination source (Fig. 4 and S8). The rate constant of the direct $E \rightarrow Z$ photoisomerization (Table 2) decreases with increasing the solvent polarity and goes from $38 \cdot 10^{-3}$ s^{-1} in chloroform to $6 \cdot 10^{-3}$ s^{-1} in ethanol for compound **4c**. The same trend is observed for compound **4d** whose isomerization constant decreased from $29 \cdot 10^{-3}$ s^{-1} in chloroform to $5 \cdot 10^{-3}$ s^{-1} in ethanol. The highest rate constant for the photoinduced back-switch reaction was obtained in ethanol amounting at $222 \cdot 10^{-3}$ s^{-1} and $192 \cdot 10^{-3}$ s^{-1} for compounds **4c** and **4d**, respectively. The kinetic constants appear to be independent of the donor character.

On the other hand, the thermal back-switch is extremely slow at both 25 °C, and 40 °C, with no conversion detected within six months. All these results agree with those presented in our previous studies dealing with compounds **4a** and **4b**. [33–34].

The direct photoisomerization quantum yields have been determined by UV/vis spectroscopy (as described in the experimental part 5.6) and validated for compounds **4a** and **4b** (Fig. S9) by independent *in-situ* NMR measurements (as described in the experimental part 5.7). The results presented in Table 2 show that the direct quantum yields depend on the solvent's polarity being approximately 2 to 5 times larger in chloroform than in ethanol (On the contrary, the inverse quantum yields are largely independent of the solvent polarity for an alkoxy donor moiety. However, they are twice as high in ethanol as in chloroform for an amine donor moiety. The quantum yield of reverse photoisomerization is comprised between 1.5 and 5 times those of the direct switch, as it was estimated from *Z*-isomers absorbance spectra (see experimental part, Figs. S10-S13 and Table S2). Finally, those values are lower than those reported for similar stilbenes derivatives ($\Phi_{EZ} = 0.2$–0.6, $\Phi_{ZE} = 0.3$–0.5) [43–44] or azobenzenes ($\Phi_{EZ} = 0.1$–0.5, $\Phi_{ZE} = 0.2$–0.6). [45–46].

Table 2
E/Z ratios and photoisomerization kinetics of the **4a-4d** series at the PPS state after irradiation at 375 nm (PSS1 direct), then at 300 nm (PSS2 back switch) The photoisomerization quantum yield for the direct and backward process are also reported. For **4a** and **4b** in DMSO, independent in-situ NMR measurements provided identical $\Phi_{E/Z}/\Phi_{Z/E}$ quantum yields.

	Solvent	*E/Z* (AS)[a]	*E/Z* (PSS1)[a]	*E/Z* (PSS2)[a]	$k^{375}_{E\to Z}\cdot 10^3$ (s^{-1}) by UV	$k^{300}_{Z\to E}\cdot 10^3$ (s^{-1}) by UV	$k^{nr}_{Z\to E}\cdot 10^n$ (s^{-1}) by UV [b]	φ_{EZ} / $\varphi_{ZE}$by UV
4a	$CHCl_3$	n.d.	n.d.	n.d.	30	127	1,6	n.d. / n.d.
	MeCN	n.d.	n.d.	n.d.	18	124	<1	n.d. / n.d.
	DMSO	100/0	47/53	64/36	12	182	<1	0.08 / 0.47[c]
	EtOH	92/8	25/75	64/36	16	145	4.4	0.10 / 0.08
4b	$CHCl_3$	98/2	25/75	70/30	27	200	0	0.17 / 0.19
	MeCN	97/3	16/84	47/53	18	150	0	0.12 / 0.15
	DMSO	95/5	50/50	85/15	6	106	0	0.05 / 0.13[c]
	EtOH	95/5	35/65	60/40	10	224	0	0.07 / 0.17
4c	$CHCl_3$	98/2	20/80	54/46	38	211	0	0.25 / 0.23
	MeCN	97/3	20/80	60/40	22	177	0	0.16 / 0.23
	DMSO	96/4	50/50	85/15	10	109	0	0.08 / 0.25
	EtOH	97/3	47/53	80/20	6	222	0	0.06 / 0.19
4d	$CHCl_3$	96/4	25/75	Degrad.	29	Degrad.	0	0.20 / 0.13
	MeCN	97/3	47/53	85/15	13	185	0	0.09 / 0.17
	DMSO	97/3	63/37	83/17	10	117	0	0.07 / 0.25
	EtOH	95/5	84/16	95/5	5	192	0	0.04 / 0.25

[a] As determined from NMR measurements.
[b] At 25 °C, as determined within six months.
[c] Confirmed by in-situ NMR measurements. NB. All samples contain 1v/v% DMSO.

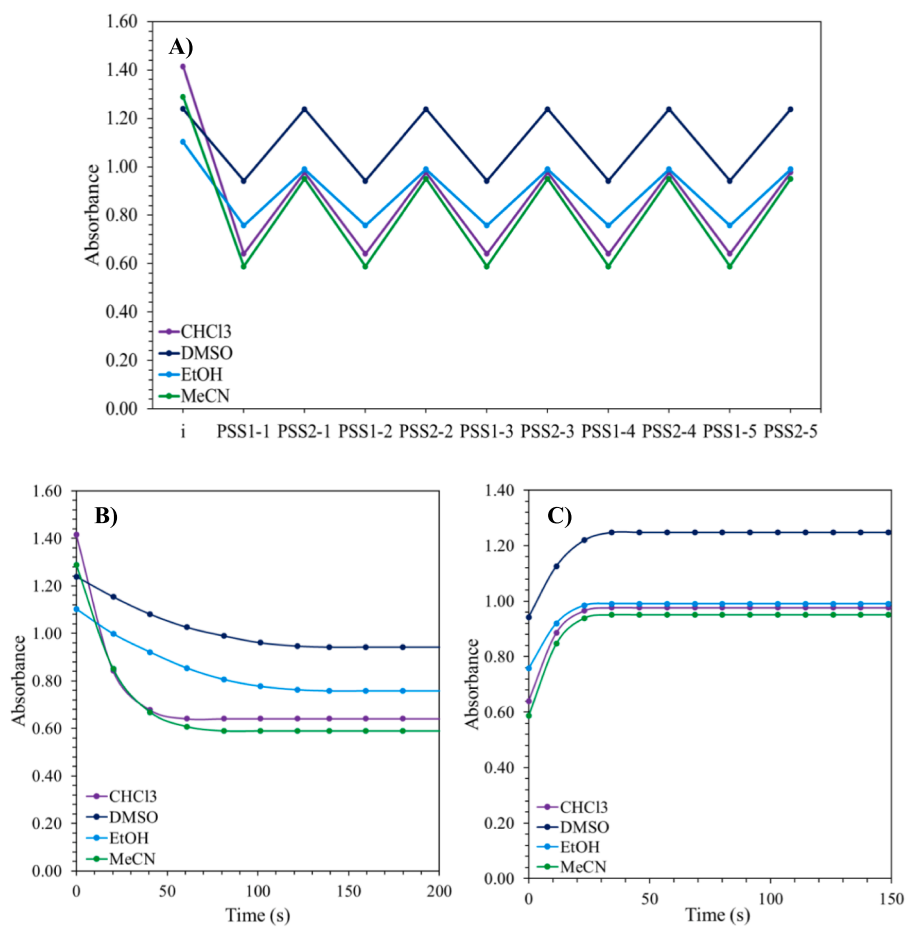

Fig. 4. Absorbance of **4c** at λ^{max} during 5 cycles of successive irradiation at two different wavelengths, 375 nm (1.5 W, 10 s) and 300 nm (350 mW, 30 s) (A), evolution of the absorbance during the photoisomerization process at 375 nm (B) and 300 nm (C) as a function of time.

Interestingly, absolutely no evidence of photoisomerization has been detected for the series **6a-6d**, neither by NMR nor UV/Vis. Thus, the existence of competitive relaxation channels was considered. For these reasons, and due to the relevance of PTT, the photoinduced temperature increase was monitored for this series of compounds (Fig. 5).

2.4. *Photothermal properties of the **6a-6d** series*

The existence of light activated floppy intramolecular motions such as rotation, vibration, and twisting promote effective non-radiative decay and releases the excitation energy as heat. The photothermal

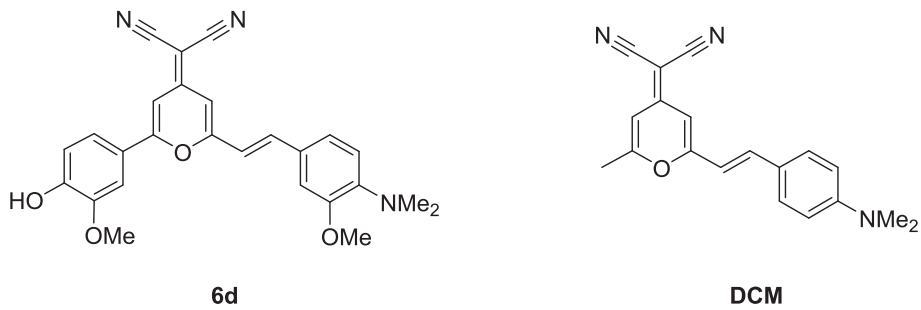

Fig. 5. Structures of compound **6d** and commercially available DCM.

properties were studied through the photothermal conversion efficiency (η) obtained by monitoring the time-evolution of the temperature under laser irradiation at 470 nm with an irradiance of 0.68 W•cm^{-2} (Fig. 6 and Figs. S14–S16) and the absorption spectra of each compound at the beginning of each photothermal cycle. From those results, it is clear that a photothermal effect is operative and that a correlation exists between the maximum temperature achieved and the donor character of the peripheral group. Indeed, the temperature of the solutions of compounds **6a-c** raises from 25 °C to 49–53 °C after 400 s irradiation of a 40 μM solution (Fig. 6-A), while the temperature of irradiated pure DMSO increased by only 1.5 °C under the same conditions. The temperature rise of **6d** was even more important reaching 72 °C for a 40 μM solution (Fig. 6-A). It should also be noted that no photothermal effect was observed in the case of the **4a-d** series, for which the photoisomerization remained the favored deexcitation pathway.

Since no similar structure molecule is referenced in the literature for its photothermal properties, the commercially available 4-dicyanomethylene-2-methyl-6-(*p*-dimethylamino-styryl)-4H-pyran (DCM, Fig. 6) was studied under the same conditions of concentration and irradiance. Upon irradiation, the temperature initially increases to reach a maximum of ΔT = 30 °C then decreases after 300 s irradiation time (Fig. 6-B).

As expected, the temperature increase is concentration and laser-power dependent. The temperature increase changed from 6.8 °C to 27 °C and from 10.9 °C to 45.5 °C for compounds **6a-c** and **6d**, respectively, increasing the concentration from 5 to 40 μM (Fig. 6-C). Similarly, the temperature increases almost doubled when multiplying the laser intensity by a factor 2 (1.36 W•cm^{-2}) (Fig. 6).

The photothermal conversion efficiency (η) was determined from equation (12) (see experimental part). Table 3 shows similar values of η for all **6a-c** compounds of about 28 %, while the efficiency of **6d**, which bears a stronger dimethylamine donor group, almost doubled reaching 50 %. The latest is also definitely more efficient than DCM, whose η was estimated to 28 %.

To further evaluate the potential of those molecules as PTT agents, the resistance to photothermal fatigue was determined. To do so, 20 μM solutions in DMSO have been irradiated under the same conditions, and the absorption spectra were recorded during 5 cycles. All **6a-d** compounds present good photostability as their temperature gain (ΔT) remains slightly constant with a decrease of only 10 % after 5 cycles (Fig. 7-A) while DCM recorded a decrease of 52 % after one cycle and of 72 % after 5 cycles (Fig. 7-B). UV–vis analyses revealed a slight chemical modification of compounds **6a-d** (Fig. 7-C and S17), either due to photodegradation or to photoisomerization under high irradiance. DCM exhibits even more dramatic evolution of the UV–vis spectrum (Fig. 7-D), probably due to its isomerization, as already reported in the literature or to a higher photodegradation. [47] This also leads to the diminution over irradiation time of the DCM absorption at irradiation wavelength (470 nm), which contribute to its lower photothermal conversion efficiency as compared to **6d**.

2.5. Photoisomerization vs photothermy rationalized by molecular modeling

To properly rationalize the different behavior observed by the two distinctive series of compounds, namely photoisomerization and photothermal conversion, we resorted to the exploration of the most relevant potential energy surfaces (PES). Importantly and as pictorially represented in Fig. 8, the inclusion of the malonitrile group formally adds up a novel degree of freedom to be considered. This is due to the activation of the rotation of the malonitrile moiety in the excited state, which may be regarded as a consequence of consecutive isomerizations of the $=C(CN)_2$ double bond.

Coherently with what was already observed for **4a** and CC, [35,48] the inclusion of a donor group in **4d** only slightly modifies the topology of the PES (Fig. 8A). In particular we can observe that the isomerization of the ethynyl double bond is possible through a conical intersection which can be reached on both the n-π* and the π-π* state. However, the path going through the latter state appears more favorable and should result in a faster process and higher efficiency. Nevertheless, a barrier is present on both surfaces, as was the case for natural CC, **4a**, and **4d**, which should prevent an ultrafast isomerization and globally lowers the quantum yields. However, the stabilization of the π-π* state over the n-π* state, whatever the polarity of the environment, is also coherent with the observed slight solvent-dependence of the photoisomerization quantum yield.

On the other hand, the PES of **6a,d** (Fig. 8B) are strikingly different. Indeed, we can see that isomerization of the ethynyl bond, while still possible and still involving a S_1/S_0 conical intersection requires a much higher barrier than for **4a,d**, which mainly blocks this channel. Contrarily, we can observe an almost barrierless pathway which leads to a second S_1/S_0 conical intersection involving the rotation around the malonitrile bond. Interestingly, this pathway is not only barrierless but also crosses the one leading to the ethylenic isomerization. Consequently, the inclusion of the malonitrile groups offers a novel decay path which involves the activation of the rotation mode of the CN peripheral groups. Such a relaxation can be assimilated to the activation of rotationally based energy dissipation channels and is hence coherent with the observed photothermal effects. In addition, a similar path is obtained for **6d** showing that the donor group has virtually a minor influence on the photochemistry in comparison with the malonitrile addition. In this, even a stepper decay is observed yielding to a slightly shifted isomerization angle.

3. Conclusions

We have designed and synthesized two families of chromophores for potential therapeutic applications. They are based on γ-pyrone CC analogs presenting different electron-donating (hydroxy, alkoxy, amine) and electron-attracting (oxo, malonitrile) groups and absorbing in the UV–vis window. Molecular modeling has shown that the topology of the most relevant PES is highly affected by the choice of the later substituent and that the presence of a malonitrile group opens totally new relaxation

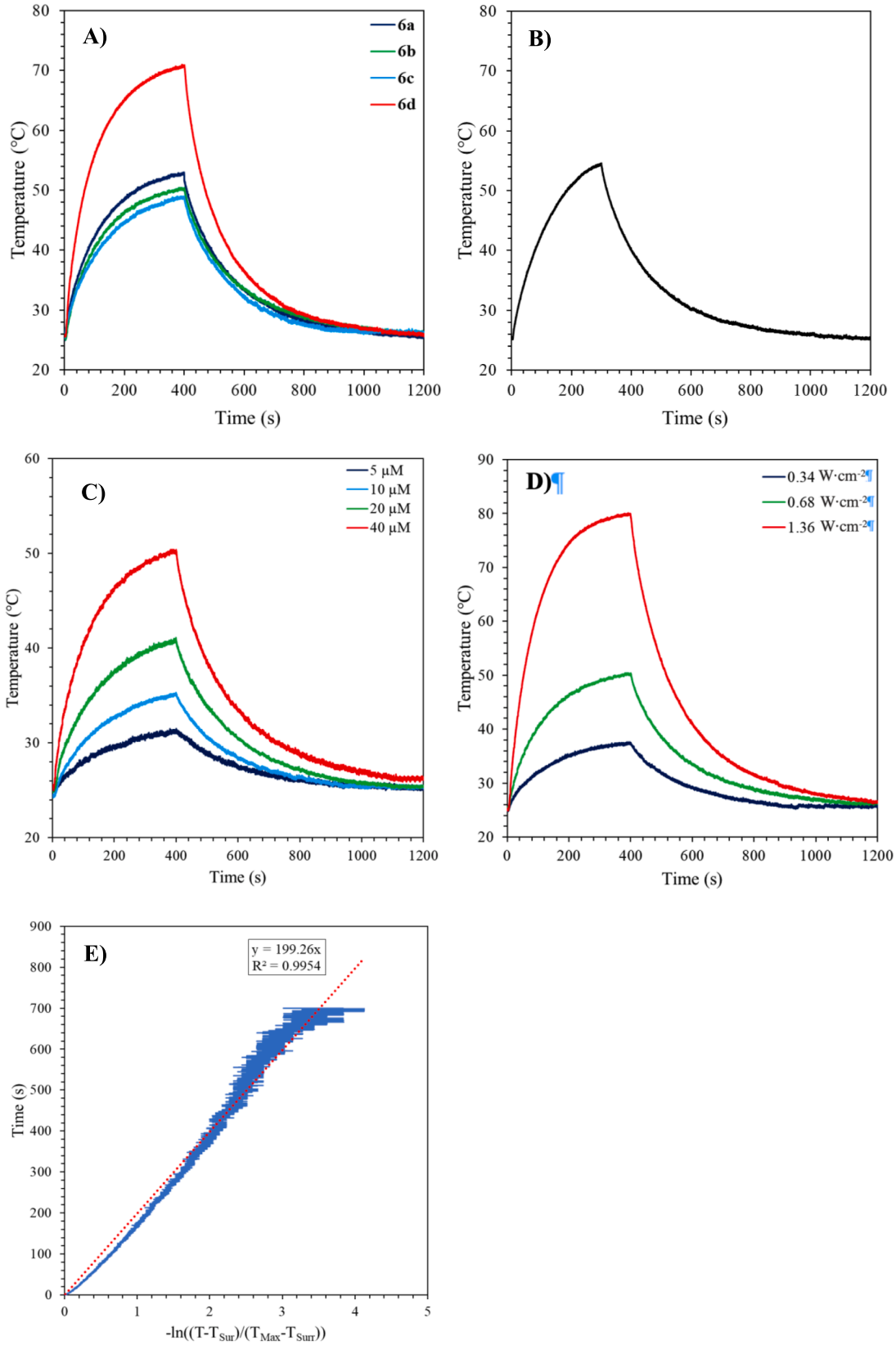

Fig. 6. Photothermal properties of compounds **6a-d** and DCM. Temperature evolution of a 40 µM solution of **6a-d** (A) and commercial DCM (B) during an on/off cycle through irradiation at 470 nm (0.68 W•cm^{-2}). Temperature evolution of a **6b** solutions at various concentrations during an on/off cycle irradiation at 470 nm (0.68 W•cm^{-2}) (C). Temperature evolution of a 40 µM solutions of **6b** during an on/off cycle at 470 nm irradiation performed with various irradiance (D). Determination of the time constant τ_s for compound **6b**, 20 µM, 0.68 W•cm^{-2} (E).

Table 3
Photothermal properties of compounds **6a-d** and commercial DCM at 20 μM in DMSO.

	6a	6b	6c	6d	DCM
A_{470}	0.371	0.335	0.282	0.36	0.539
$T_{Max} - T_{Surr}(°C)$	19.5	17	15.9	31.5	20.7
$\tau_s(s)$	171.6	199.3	184.7	184.1	184.9
$hS(mW\bullet°C^{-1})$	2.45	2.11	2.28	2.28	2.27
$\eta(\%)$	32	25	28	50	25

pathways driven by the photoactivated rotation of CN groups, efficiently competing with the ethylenic double bond isomerization. Consequently, two different photochemical effects are expected for the two distinct families. Indeed, we have shown that the keto compounds provide efficient photoswitches through the *E/Z* isomerization of the ethynyl double bond at 375 nm irradiation. The back-switch allows the partial recovery of the favorable *E* isomer by irradiation at 300 nm, still prevented thermally. The oxo compounds also showed excellent fatigue resistance properties at least over 5 cycles. Malonitrile bearing compounds are instead not isomerizing but behaves as excellent PTT agents. Indeed, irradiation at 470 nm in DMSO leads to a temperature increase up to more than 50 °C for compounds **6a-c** and more than 70 °C for **6d**. Moreover, this temperature rise is proportional to the chromophore concentration and the laser irradiance. All the compounds present attractive photothermal conversion efficiencies ranging from 28 % to 50 % and good photothermal resistance. Hence, we believe that our molecular design has highlighted the competition between the different relaxation pathways: fluorescence, isomerization, and heat production. More importantly, we have shown how the precise choice of the peripheral substituents may favor one relaxation channel, hence driving and tuning a proper photochemical response. The possibility of obtaining biomimetic photoswitches or photothermal agents with well-defined properties indicates that our two families of compounds are promising for further applications in the biomedical field especially due to their non negligible cross section in absorbing two photons in the NIR region. [34–35] Indeed, irradiation in the optical biological window is

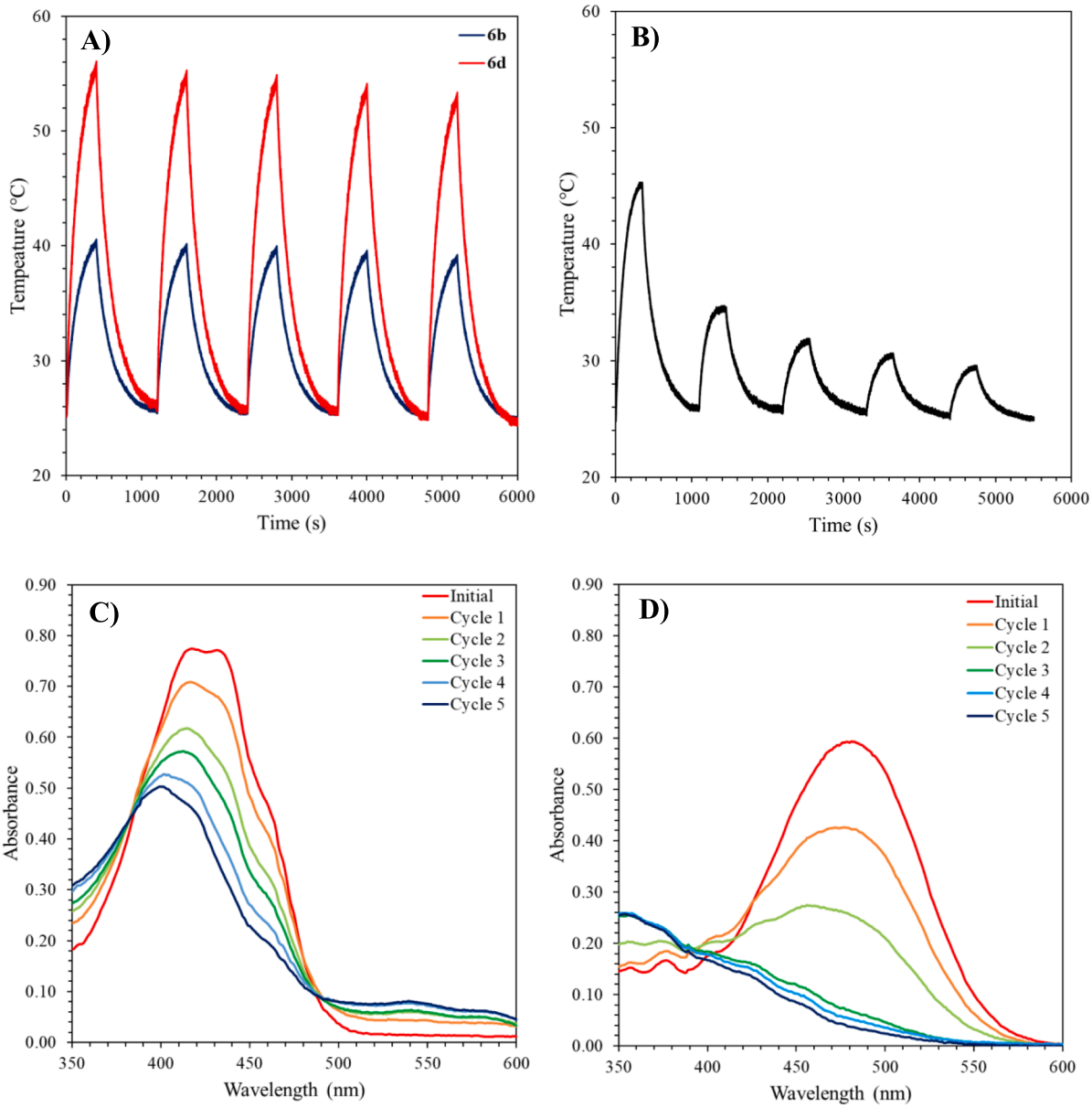

Fig. 7. Temperature evolution of a 20 μM solution of **6b** and **6d** (A), and commercial DCM (B) in DMSO as function of time, during 5 on/off cycles of irradiation at 470 nm (0.68 W•cm^{-2}). Absorption spectra of compound **6b** (C) and DCM (D) between each irradiation cycle.

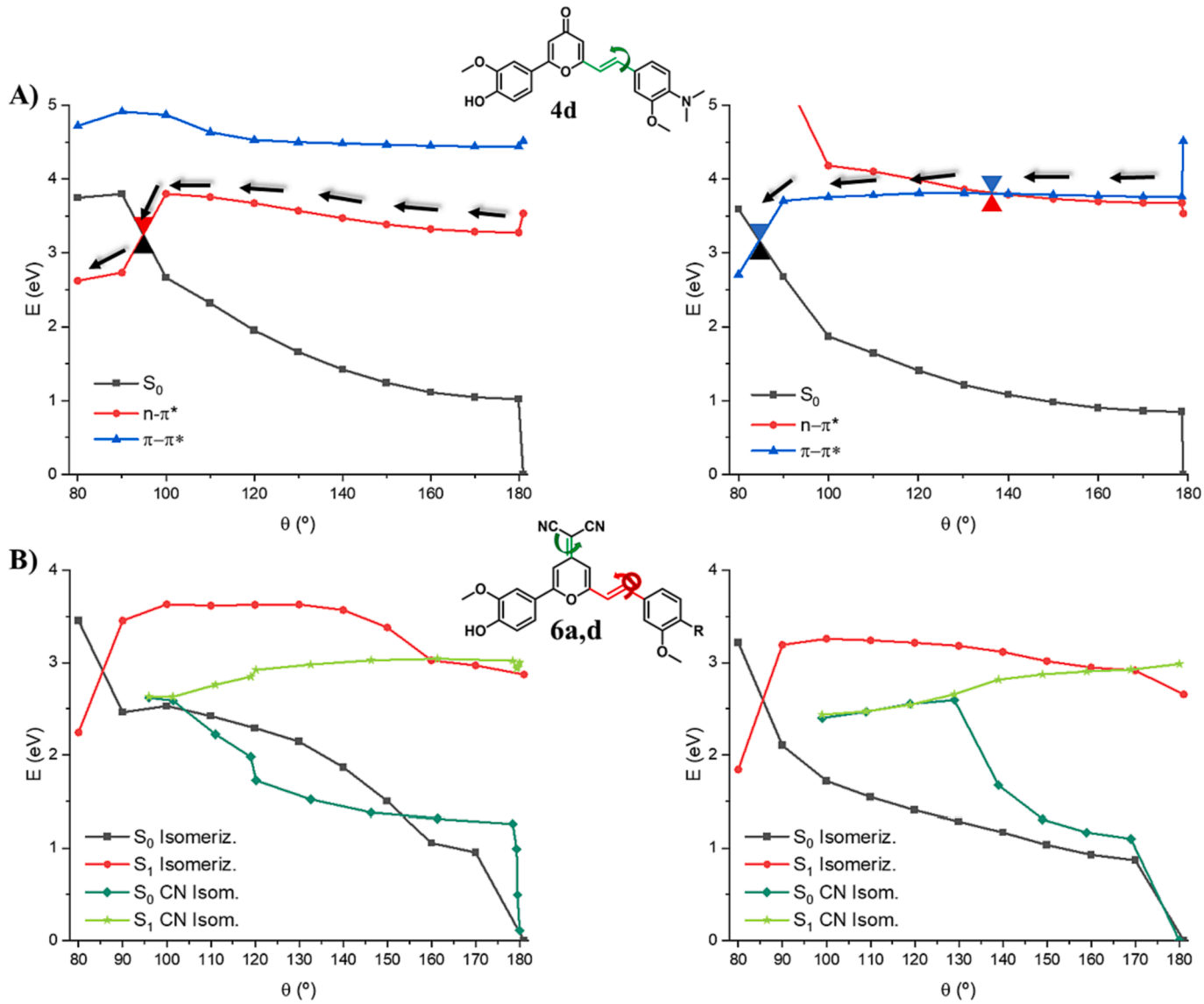

Fig. 8. PES for the photoisomerization through the n-π* (right) and π-π* (left) for compound **4d** (A). PES showing the competition between photoisomerization and the activation of the malonitrile rotation for **6a** (B, left) and **6d** (B, right). Most important degrees of freedom for **4d** as well as **6a** and **6d** are represented in green while the unfavorable degrees of freedom are in red for each system.

compulsory for therapeutical applications, to prevent high energy per photon UV–vis irradiation which is detrimental to cell tissues and has low penetration depth. Moreover, some antennas system to switch absorption in the visible or infrared portion of the spectrum could also be considered.

It should be also noted that those compounds need further modifications and characterizations before being used as compounds with potential therapeutic applications. This includes formulation or chemical grafting of hydrophilic moieties to reach adequate solubility in the aqueous medium, and studies of their specific interaction with biological systems, toxicity (in dark condition and under illumination) or biodistribution.

4. Experimental section

4.1. General

All reactions were carried out under argon atmosphere. Other solvents and liquid reagents were purified and dried according to recommended procedures. The chemical reagents were purchased from Merck, Fisher Scientific, or Sigma-Aldrich and were used as received. Analytical TLC analyses were performed using standard procedures on silica gel 60 F254 plates (Merck). The compounds were visualized with UV light (254 nm), and alternatively, potassium permanganate aqueous solution was used. Silica gel column chromatography was performed on a glass column filled with silica gel (63–200 μm) (Merck). The melting points (mp) were determined with a Tottoli apparatus and are uncorrected. Spectroscopic analyses and kinetic measurements were carried out on the PhotoNS Platform of the L2CM Laboratory, University of Lorraine. FTIR spectra were recorded on a Shimadzu IRAffinity-1 apparatus equipped with ATR PIKE Technologies model GladiATR (cm^{-1}). NMR spectra were recorded at 300 K, unless stated otherwise, using a Bruker DRX400 spectrometer (400 MHz for ^{1}H and 100.6 MHz for ^{13}C). Chemical shifts are reported in ppm (δ) relative to deuterated solvent residual peaks. For complete assignment of ^{1}H and ^{13}C signals, two-dimensional ^{1}H, ^{1}H COSY and ^{1}H, ^{13}C correlation spectra were recorded. The following abbreviations are used to explain the observed multiplicities: s, singlet; d, doublet; dd, doublet of doublets; ddd, doublet of doublets of doublets; t, triplet; td, triplet of doublets; m, multiplet; and bs, broad singlet. HRMS were recorded on a microTOFQ (Bruker) ESI/

QqTOF spectrometer. Compounds **1**, [34] **2a**, [49] **2b**, [50] **2c**, [51] **2d**, [52] **3a**, [34] **3b**, [33] **4a**, [34] and **4b** [33] were synthesized according to the methods described in respective references.

4.2. Molecular modeling

CASPT2//CASSCF approach has been considered to explore the excited states PES landscape and hence characterize the photochemistry of these compounds around the isomerizable pathways [53–54].

As a first step the ground state geometry has been optimized for all compounds at DFT level using the B3LYP functional. [55] Subsequently, those geometries were used to compute the absorption spectrum as vertical excitations using CAM-B3LYP functional in the TD-DFT formalism. [56] For this kind of systems, this functional feature a proper description as previously reported, [35] even usually underestimates the π-π* transition in comparison with n-π*. The nature of the excited states has also been determined using NTO formalisms. [42] For the computation of UV–vis spectra, a Wigner distribution over the vibrational normal modes was done and 100 geometries were generated. The final spectrum was a convolution of gaussians of the single point computed transition energies using the CAM-B3LYP/6-31G*. On top of the B3LYP optimized geometry wavefunction calculations have also been performed under MS-CASPT2//SA(4)-CASSCF level of theory. [54] Firstly, CASSCF calculations including 4 averaged states (from S_0 to S_3) were done followed by a multistate 2nd order perturbation theory to the CASSCF wavefunction. As previously reported, [57] the active space containing 10 electrons in 9 orbitals (10,9) was used for compound **4d**, including the n orbital and different π and π* orbitals. In case of **6a** and **6d** the use of 8 electrons in 8 orbitals (8,8) was selected consistently with the elimination of the n orbital.

In particular, the S_1 ^{1}(n-π*) and S_2 ^{1}(π-π*) states identified at Franck–Condon were optimized at CASSCF level, reaching the respective minima whose diabatic nature was confirmed by analyzing the respective molecular orbitals. Starting from these structures, relaxed scans along the dihedral angle optimizing both S_1 and S_2 states were performed freezing the dihedral at the desired value and relaxing along all the other coordinates. In addition, the same procedure for the other compounds **6a** and **6d** was also performed. In case of **6a**, the MEP from FC yields directly to a crossing region and not scan was needed for this coordinate.

On the optimized CASSCF structures, single point multi-state CASPT2 (MS-CASPT2) were performed to include the necessary dynamic electron correlation. For those calculations, an imaginary shift of 0.2 eV without IPEA was applied to avoid the influence of intruder states.

For all calculations, the 6-31G* basis set was used. [58] CASSCF and CASPT2 calculations have been performed using the OpenMolcas suite of programs, [59–60] while DFT and TD-DFT have been obtained employing the Gaussian16 software. [61].

4.3. Synthesis

4.3.1. (E)-2-(4-(dodecyloxy)-3-methoxystyryl)-6-(3-methoxy-4-(methoxymethoxy) phenyl)-4H-pyran-4-one, 3c

To a stirred solution of 2-(3-methoxy-4-(methoxymethoxy)phenyl)-6-methyl-4H-pyran-4-one **1** (2.00 g, 7.24 mmol) and 4-dodecyloxy-3-methoxybenzaldehyde **2c** (3.44 g, 10.74 mmol, 1.48 eq.) in dry EtOH (120 mL) at room temperature was added fresh EtONa solution (1.56 M in EtOH, 10 mL, 15.6 mmol, 2.15 eq.) dropwise and the mixture was stirred 48 h at 40 °C (CCM, SiO_2, EtOAc 100 %). The reaction mixture was quenched with water (100 mL). The crude product was extracted with DCM and the organic phase was separated. The aqueous phase was further extracted with DCM (4 × 50 mL). The combined organic phase was washed with water (3 × 50 mL) and brine (3 × 50 mL) then dried over Na_2SO_4, filtered, and evaporated under reduced pressure. Chromatography on silica gel with EtOAc (100 %) afforded the title compound **3c** as a yellow solid (1.89 g, 45 %). ***R_f***: 0.38 (EtOAc 100 %). **M.p.**: 111 °C. **IR** (ATR, cm^{-1}): 2916, 2849, 1647, 1634, 1599, 1510. **UV–vis** (DMSO): 352 nm. **^{1}H NMR** (400 MHz, $CDCl_3$): δ 7.45 (dd, $J_{H,H}$ = 8.5, 2.1 Hz, 1H; Ar-H), 7.40 (d, $J_{H,H}$ = 16.0 Hz, 1H; $H_{ethyl\ \beta}$), 7.29 (m, 2H; Ar-*H*), 7.09 (m, 2H; Ar-*H*), 6.89 (d, $J_{H,H}$ = 8.1 Hz, 1H; Ar-*H*), 6.65 (d, $J_{H,H}$ = 2.2 Hz, 1H; H_{pyrone}), 6.62 (d, $J_{H,H}$ = 16.0 Hz, 1H; $H_{ethyl\ \alpha}$), 6.29 (d, $J_{H,H}$ = 2.1 Hz, 1H; H_{pyrone}), 5.32 (s, 2H; OCH_2O), 4.06 (t, $J_{H,H}$ = 6.9 Hz, 2H; OCH_2), 3.98 (s, 3H; OCH_3), 3.95 (s, 3H; OCH_3), 3.54 (s, 3H; CH_2OCH_3), 1.87 (m, 2H; OCH_2CH_2), 1.46 (m, 2H; $OCH_2CH_2CH_2$), 1.36–1.27 (m, 16H; $(CH_2)_n$), 0.88 (t, $J_{H,H}$ = 6.8 Hz, 3H; CH_2CH_3). **^{13}C {^{1}H} NMR** (100 MHz, $CDCl_3$): δ 180.5, 162.9, 162.1, 150.7, 150.1, 149.9, 149.5, 136.1, 127.9, 125.8, 122.1, 119.6, 117.7, 116.1, 113.4, 112.7, 110.7, 109.9, 109.5, 95.4, 69.3, 56.6, 56.3, 56.2, 32.1, 29.80, 29.78, 29.74, 29.70, 29.53, 29.49, 29.2, 26.1, 22.8, 14.3. **ESI-MS** (HR): *m/z* $[M+H]^+$ calcd for $C_{35}H_{47}O_7$: 579.3316, found: 579.3333; *m/z* $[M+Na]^+$ calcd for $C_{35}H_{46}NaO_7$: 601.3136, found: 601.3146; *m/z* $[M+K]^+$ calcd for $C_{35}H_{46}KO_7$: 617.2875, found: 617.2856.

4.3.2. (E)-2-(4-(dimethylamino)-3-methoxystyryl)-6-(3-methoxy-4-(methoxymethoxy) phenyl)-4H-pyran-4-one, 3d

To a stirred solution of 2-(3-methoxy-4-(methoxymethoxy)phenyl)-6-methyl-4*H*-pyran-4-one **1** (346 mg, 1.25 mmol) and 4-(dimethylamino)-3-methoxybenzaldehyde **2d** (342 mg, 1.91 mmol, 1.52 eq.) in dry EtOH (12 mL) at room temperature was added fresh EtONa solution (1.13 M in EtOH, 2 mL, 2.26 mmol, 1.80 eq.) dropwise and the mixture was stirred 48 h at 40 °C (CCM, SiO_2, EtOAc 100 %). The reaction mixture was quenched with water (10 mL). The crude product was extracted with DCM and the organic phase was separated. The aqueous phase was further extracted with DCM (4 × 10 mL). The combined organic phase was washed with water (3 × 10 mL) and brine (3 × 10 mL) then dried over Na_2SO_4, filtered, and evaporated under reduced pressure. Chromatography on silica gel with EtOAc (100 %) afforded the title compound **3d** as an orange solid (249 mg, 46 %). ***R_f***: 0.29 (EtOAc 100 %). **M.p.**: 137 °C. **IR** (ATR, cm^{-1}): 2938, 2828, 1641, 1591, 1504. **UV–vis** (DMSO): 388 nm. **^{1}H NMR** (400 MHz, $CDCl_3$): δ 7.44 (dd, $J_{H,H}$ = 8.5, 2.0 Hz, 1H; Ar-*H*), 7.40 (d, $J_{H,H}$ = 16.0 Hz, 1H; $H_{ethyl\ \beta}$), 7.30 (d, $J_{H,H}$ = 1.6 Hz, 1H; Ar-*H*), 7.28 (d, $J_{H,H}$ = 8.5 Hz, 1H; Ar-*H*), 7.09 (dd, $J_{H,H}$ = 8.1, 1.3 Hz, 1H; Ar-*H*), 7.03 (d, $J_{H,H}$ = 1.4 Hz, 1H; Ar-*H*), 6.90 (m, 1H; Ar-*H*), 6.64 (d, $J_{H,H}$ = 2.2 Hz, 1H; H_{pyrone}), 6.62 (d, $J_{H,H}$ = 15.9 Hz, 1H; $H_{ethyl\ \alpha}$), 6.27 (d, $J_{H,H}$ = 1.9 Hz, 1H; H_{pyrone}), 5.31 (s, 2H; OCH_2O), 3.97 (s, 3H; OCH_3), 3.96 (s, 3H; OCH_3), 3.53 (s, 3H; CH_2OCH_3), 2.86 (s, 6H; $N(CH_3)_2$). **^{13}C{^{1}H} NMR** (100 MHz, $CDCl_3$): δ 180.4, 162.8, 162.1, 152.3, 150.0, 149.4, 144.5, 136.2, 128.7, 125.8, 122.1, 119.5, 117.9, 117.3, 116.0, 113.2, 110.6, 109.4, 109.3, 95.3, 56.6, 56.2, 55.7, 43.1. **ESI-MS** (HR): *m/z* $[M+H]^+$ calcd for $C_{25}H_{28}NO_6$: 438.1911, found: 438.1915; *m/z* $[M+Na]^+$ calcd for $C_{25}H_{27}NNaO_6$: 460.1731, found: 460.1743.

4.3.3. (E)-2-(4-dodecyloxy-3-methoxystyryl)-6-(4-hydroxy-3-methoxyphenyl)-4H-pyran-4-one, 4c

To a stirred solution of (*E*)-2-(4-dodecyloxy-3-methoxystyryl)-6-(3-methoxy-4-(methoxymethoxy) phenyl)-4H-pyran-4-one **3c** (1.75 g, 3.02 mmol) in MeOH (100 mL) at room temperature was added an excess of HCl 2 M (8 mL, 16.00 mmol, 5.29 eq.) dropwise and the mixture was refluxed during 3 h (CCM, SiO_2, EtOAc 100 %). The reaction mixture was quenched with water (100 mL). The precipitate obtained was filtered, washed with water, and finally dried to afford the title compound **4c** as a yellow solid (1.60 g, 99 %). ***R_f***: 0.35 (EtOAc 100 %). **M.p.**: 70 °C. **IR** (ATR, cm^{-1}): 3395, 2918, 2851, 1641, 1595, 1504. **^{1}H NMR** (400 MHz, $CDCl_3$): δ 7.45 (dd, $J_{H,H}$ = 8.4, 2.0 Hz, 1H; Ar-*H*), 7.40 (d, $J_{H,H}$ = 16.0 Hz, 1H; $H_{ethyl\ \beta}$), 7.26 (d, $J_{H,H}$ = 2.1 Hz, 1H; Ar-*H*), 7.10 (dd, $J_{H,H}$ = 8.4, 2.0 Hz, 1H; Ar-*H*), 7.08 (d, $J_{H,H}$ = 2.0 Hz, 1H; Ar-*H*), 7.07 (d, $J_{H,H}$ = 8.4 Hz, 1H; Ar-*H*), 6.89 (d, $J_{H,H}$ = 8.0 Hz, 1H; Ar-*H*), 6.63 (d, $J_{H,H}$ = 2.2 Hz, 1H; H_{pyrone}), 6.62 (d, $J_{H,H}$ = 16.0 Hz, 1H; $H_{ethyl\ \alpha}$), 6.29 (d, $J_{H,H}$ = 2.1 Hz, 1H; H_{pyrone}), 4.05 (t, $J_{H,H}$ = 6.9 Hz, 2H; OCH_2), 3.99 (s, 3H; OCH_3), 3.94 (s, 3H; OCH_3), 1.86 (m, 2H; OCH_2CH_2), 1.47

(m, 2H; $OCH_2CH_2CH_2$), 1.38–1.24 (m, 16H; $(CH_2)_n$), 0.88 (t, $J_{H,H}$ = 6.8 Hz, 3H; CH_2CH_3). **$^{13}C\{^1H\}$ NMR** (100 MHz, $CDCl_3$): δ 180.5, 163.2, 162.1, 150.7, 149.9, 149.0, 147.1, 136.1, 127.9, 123.9, 122.2, 120.3, 117.7, 115.2, 113.3, 112.7, 110.2, 109.9, 108.4, 69.3, 56.3, 56.2, 32.1, 29.80, 29.78, 29.73, 29.69, 29.53, 29.49, 29.2, 26.1, 22.8, 14.3. **ESI-MS** (HR): *m/z* $[M+H]^+$ calcd for $C_{33}H_{43}O_6$: 535.3054, found: 535.3092; *m/z* $[M+Na]^+$ calcd for $C_{33}H_{42}NaO_6$: 557.2874, found: 557.2899; *m/z* $[M+K]^+$ calcd for $C_{33}H_{42}KO_6$: 573.2613, found: 573.2570.

4.3.4. (Z)-2-(4-dodecyloxy-3-methoxystyryl)-6-(4-hydroxy-3-methoxyphenyl)-4H-pyran-4-one, 4c'

An irradiation at 375 nm of the solution of **4c** in DMSO led to **4c'** with a ratio: **4c/4c'** 50:50. **^1H NMR** (400 MHz, $CDCl_3$): δ 6.93 (dd, $J_{H,H}$ = 8.3, 1.6 Hz, 1H; Ar-*H*), 6.88–6.82 (m, 5H; Ar-$H + H_{ethyl\ \beta}$), 6.76 (d, $J_{H,H}$ = 8.3 Hz, 1H; Ar-*H*), 6.63 (d, $J_{H,H}$ = 2.2 Hz, 1H; H_{pyrone}), 6.33 (d, $J_{H,H}$ = 2.1 Hz, 1H; H_{pyrone}), 6.17 (d, $J_{H,H}$ = 12.3 Hz, 1H; $H_{ethyl\ \alpha}$), 6.07 (br s, 1H; O*H*), 3.97 (t, $J_{H,H}$ = 6.7 Hz, 2H; OCH_2CH_2), 3.70 (s, 3H; OCH_3), 3.65 (s, 3H; OCH_3), 1.81 (m, 2H; OCH_2CH_2), 1.44 (m, 2H; $OCH_2CH_2CH_2$), 1.35–1.24 (m, 16H; $(CH_2)_n$), 0.88 (t, $J_{H,H}$ = 6.8 Hz, 3H; CH_2CH_3). **$^{13}C\{^1H\}$ NMR** (100 MHz, $CDCl_3$): δ 180.3, 163.4, 162.1, 149.5, 149.2, 149.0, 146.9, 138.1, 128.5, 123.0, 122.6, 120.3, 119.3, 115.5, 114.9, 112.5, 112.4, 109.9, 108.1, 69.2, 56.00, 55.97, 32.1, 29.80, 29.78, 29.74, 29.70, 29.53, 29.49, 29.2, 26.1, 22.8, 14.3. **ESI-MS** (HR): *m/z* $[M+H]^+$ calcd for $C_{33}H_{43}O_6$: 535.3054, found: 535.3097; *m/z* $[M+Na]^+$ calcd for $C_{33}H_{42}NaO_6$: 557.2874, found: 557.2864; *m/z* $[M+K]^+$ calcd for $C_{33}H_{42}KO_6$: 573.2613, found: 573.2577.

4.3.5. (E)-2-(4-(dimethylamino)-3-methoxystyryl)-6-(4-hydroxy-3-methoxyphenyl)-4H-pyran-4-one, 4d

To a stirred solution of (*E*)-2-(4-(dimethylamino)-3-methoxystyryl)-6-(3-methoxy-4-(methoxymethoxy)phenyl)-4H-pyran-4-one **3d** (200 mg, 0.46 mmol) in MeOH (20 mL) at room temperature was added an excess of HCl 1 M (2 mL, 4.00 mmol, 8.75 eq.) dropwise and the mixture was refluxed during 3 h (CCM, SiO_2, EtOAc/MeOH 95:5). The reaction mixture was quenched with water (10 mL). The precipitate obtained was filtered, washed with water, and finally dried to afford the title compound **4d** as an orange solid (150 mg, 83 %). ***Rf***: 0.33 (EtOAc/MeOH 95:5). **M.p.**: 158 °C. **IR** (ATR, cm^{-1}): 3234 (br), 2970, 1641, 1557, 1506. **^1H NMR** (400 MHz, DMSO-d_6): δ 9.80 (s, 1H; O*H*), 7.55 (dd, $J_{H,H}$ = 8.3, 2.1 Hz, 1H; Ar-*H*), 7.49 (d, $J_{H,H}$ = 16.1 Hz, 1H; $H_{ethyl\ \beta}$), 7.48 (d, $J_{H,H}$ = 2.1 Hz, 1H; Ar-*H*), 7.30 (d, $J_{H,H}$ = 1.8 Hz, 1H; Ar-*H*), 7.22 (dd, $J_{H,H}$ = 8.3, 1.8 Hz, 1H; Ar-*H*), 7.01 (d, $J_{H,H}$ = 16.1 Hz, 1H; $H_{ethyl\ \alpha}$), 6.96 (d, $J_{H,H}$ = 8.3 Hz, 1H; Ar-*H*), 6.86 (d, $J_{H,H}$ = 8.3 Hz, 1H; Ar-*H*), 6.82 (d, $J_{H,H}$ = 2.2 Hz, 1H; H_{pyrone}), 6.29 (d, $J_{H,H}$ = 2.2 Hz, 1H; H_{pyrone}), 3.90 (s, 3H; OCH_3), 3.87 (s, 3H; OCH_3), 2.78 (s, 6H; $N(CH_3)_2$). **$^{13}C\{^1H\}$ NMR** (100 MHz, DMSO-d_6): δ 178.9, 162.1, 161.6, 151.4, 150.0, 148.0, 143.7, 135.4, 128.0, 122.1, 122.0, 119.6, 117.2, 117.0, 115.8, 112.2, 110.3, 109.8, 108.7, 55.8, 55.5, 42.3. **ESI-MS** (HR): *m/z* $[M+H]^+$ calcd for $C_{23}H_{24}NO_5$: 394.1649, found: 394.1684; *m/z* $[M+Na]^+$ calcd for $C_{23}H_{23}NNaO_5$: 416.1468, found: 416.1478.

4.3.6. (Z)-2-(4-(dimethylamino)-3-methoxystyryl)-6-(4-hydroxy-3-methoxyphenyl)-4H-pyran-4-one, 4d'

An irradiation at 375 nm of the solution of **4d** in DMSO led to **4d'** with a ratio: **4d/4d'** 63:37. **^1H NMR** (400 MHz, DMSO-d_6): δ 9.70 (s, 1H; O*H*), 6.98 (d, $J_{H,H}$ = 1.9 Hz, 1H; Ar-*H*), 6.93 (d, $J_{H,H}$ = 1.9 Hz, 1H; Ar-*H*), 6.92 (d, $J_{H,H}$ = 12.2 Hz, 1H; $H_{ethyl\ \beta}$), 6.91 (m, 1H; Ar-*H*), 6.80 (d, $J_{H,H}$ = 2.2 Hz, 1H; H_{pyrone}), 6.79 (dd, $J_{H,H}$ = 7.9, 2.3 Hz, 1H; Ar-*H*), 6.67 (dd, $J_{H,H}$ = 8.4, 1.9 Hz, 1H; Ar-*H*), 6.62 (d, $J_{H,H}$ = 8.4 Hz, 1H; Ar-*H*), 6.31 (d, $J_{H,H}$ = 2.0 Hz, 1H; H_{pyrone}), 6.30 (d, $J_{H,H}$ = 12.6 Hz, 1H; $H_{ethyl\ \alpha}$), 3.58 (s, 3H; OCH_3), 3.53 (s, 3H; OCH_3), 2.69 (s, 6H; $N(CH_3)_2$). **$^{13}C\{^1H\}$ NMR** (100 MHz, DMSO-d_6): δ 178.8, 162.3, 161.5, 150.8, 149.8, 147.7, 142.5, 137.6, 128.8, 122.3, 121.4, 119.4, 118.9, 117.0, 115.3, 114.8, 112.3, 109.2, 108.8, 56.3, 56.2, 42.3. **ESI-MS** (HR): *m/z* $[M+H]^+$ calcd for $C_{23}H_{24}NO_5$: 394.1649, found: 394.1664; *m/z* $[M+Na]^+$ calcd for $C_{23}H_{23}NNaO_5$: 416.1468, found: 416.1453.

4.3.7. (E)-4-(2-(6-(4-acetoxy-3-methoxyphenyl)-4-(dicyanomethylene)-4H-pyran-2-yl)vinyl)-2-methoxyphenylacetate, 5a

To a stirred solution of (*E*)-2-(4-hydroxy-3-methoxyphenyl)-6-(4-hydroxy-3-methoxystyryl)-4H-pyran-4-one **4a** (15 mg, 40.6 μmol) in Ac_2O (5 mL) at room temperature was added malononitrile (14 mg, 0.21 mmol, 5.17 eq.) and the mixture was refluxed at 140 °C during 2 h (CCM, SiO_2, Cyclohexane/EtOAc 1:1). The reaction mixture was cooled to room temperature and then quenched with water (5 mL). Under stirring conditions, Na_2CO_3 (1 M) was added to the mixture in batches and the pH value of the mixture was adjusted to 7. The crude product was extracted with DCM and the organic phase was separated. The aqueous phase was further extracted with DCM (4 × 10 mL). The combined organic phase was washed with water (3 × 10 mL) and brine (3 × 10 mL) then dried over Na_2SO_4, filtered, and evaporated under reduced pressure. Chromatography on silica gel with Cyclohexane/EtOAc 1:1 afforded the title compound **5a** as a brown solid (18.1 mg, 89 %). ***Rf***: 0.29 (Cyclohexane/EtOAc 1:1). **M.p.**: 232 °C. **IR** (ATR, cm^{-1}): 2918, 2208, 1751, 1642, 1592, 1507. **UV–vis** (DMSO): 417 nm. **^1H NMR** (400 MHz, $CDCl_3$): δ 7.48 (dd, $J_{H,H}$ = 8.4, 2.1 Hz, 1H; Ar-*H*), 7.46 (d, $J_{H,H}$ = 16.2 Hz, 1H; $H_{ethyl\ \beta}$), 7.35 (d, $J_{H,H}$ = 1.9 Hz, 1H; Ar-*H*), 7.23 (d, $J_{H,H}$ = 8.3 Hz, 1H; Ar-*H*), 7.13 (m, 3H; Ar-*H*), 7.04 (d, $J_{H,H}$ = 1.9 Hz, 1H; H_{pyrone}), 6.79 (d, $J_{H,H}$ = 1.9 Hz, 1H; H_{pyrone}), 6.75 (d, $J_{H,H}$ = 16.0 Hz, 1H; $H_{ethyl\ \alpha}$), 3.95 (s, 3H; OCH_3), 3.91 (s, 3H; OCH_3), 2.36 (s, 3H; $OCCH_3$), 2.34 (s, 3H; $OCCH_3$). **$^{13}C\{^1H\}$ NMR** (100 MHz, $CDCl_3$): δ 165.9, 165.7, 159.4, 158.5, 155.9, 152.1, 151.8, 143.3, 141.9, 137.7, 133.5, 129.3, 124.0, 123.7, 121.4, 119.6, 118.6, 115.1, 110.9, 110.2, 107.8, 104.5, 60.8, 56.4, 56.2, 20.8. **ESI-MS** (HR): *m/z* $[M+H]^+$ calcd for $C_{28}H_{27}N_2O_5$: 471.1914, found: 471.1955; *m/z* $[M+Na]^+$ calcd for $C_{28}H_{26}N_2NaO_5$: 493.1734, found: 493.1685.

4.3.8. (E)-4-(6-(4-butoxy-3-methoxystyryl)-4-(dicyanomethylene)-4H-pyran-2-yl)-2-methoxyphenyl acetate, 5b

To a stirred solution of (*E*)-2-(4-butoxy-3-methoxystyryl)-6-(4-hydroxy-3-methoxyphenyl)-4H-pyran-4-one **4b** (1.30 mg, 3.08 mmol) in Ac_2O (100 mL) at room temperature was added malononitrile (1.00 g, 15.14 mmol, 4.92 eq.) and the mixture was refluxed at 140 °C during 3 h (CCM, SiO_2, DCM 100 %). The reaction mixture was cooled to room temperature and then quenched with water (100 mL). Under stirring conditions, Na_2CO_3 (1 M) was added to the mixture in batches and the pH value of the mixture was adjusted to 7. The crude product was extracted with DCM and the organic phase was separated. The aqueous phase was further extracted with DCM (4 × 50 mL). The combined organic phase was washed with water (3 × 50 mL) and brine (3 × 50 mL) then dried over Na_2SO_4, filtered, and evaporated under reduced pressure. Chromatography on silica gel with DCM 100 % afforded the title compound **5b** as a brown solid (1.49 mg, 94 %). ***Rf***: 0.27 (DCM 100 %). **M.p.**: 179 °C. **IR** (ATR, cm^{-1}): 2911, 2209, 1759, 1641, 1589, 1506, 1497. **UV–vis** (DMSO): 404 nm. **^1H NMR** (400 MHz, $CDCl_3$): δ 7.50 (dd, $J_{H,H}$ = 8.3, 2.0 Hz, 1H; Ar-*H*), 7.45 (d, $J_{H,H}$ = 15.9 Hz, 1H; $H_{ethyl\ \beta}$), 7.36 (d, $J_{H,H}$ = 1.9 Hz, 1H; Ar-*H*), 7.23 (d, $J_{H,H}$ = 8.4 Hz, 1H; Ar-*H*), 7.11 (dd, $J_{H,H}$ = 8.3, 1.8 Hz, 1H; Ar-*H*), 7.08 (d, $J_{H,H}$ = 1.8 Hz, 1H; Ar-*H*), 7.03 (d, $J_{H,H}$ = 1.9 Hz, 1H; H_{pyrone}), 6.91 (d, $J_{H,H}$ = 8.3 Hz, 1H; Ar-*H*), 6.76 (d, $J_{H,H}$ = 1.9 Hz, 1H; H_{pyrone}), 6.66 (d, $J_{H,H}$ = 15.9 Hz, 1H; $H_{ethyl\ \alpha}$), 4.08 (t, $J_{H,H}$ = 6.8 Hz, 2H; OCH_2CH_2), 3.96 (s, 3H; OCH_3), 3.95 (s, 3H; OCH_3), 2.36 (s, 3H; $OC(O)CH_3$), 1.86 (m, 2H; $OCH_2CH_2CH_2$), 1.51 (m, 2H; CH_2CH_3), 0.99 (t, $J_{H,H}$ = 7.4 Hz, 3H; CH_2CH_3). **$^{13}C\{^1H\}$ NMR** (100 MHz, $CDCl_3$): δ 165.7, 159.3, 159.2, 156.1, 152.1, 151.4, 150.0, 143.3, 138.6, 129.5, 127.4, 124.0, 122.9, 119.6, 116.0, 115.3, 112.6, 110.2, 109.9, 107.0, 104.4, 69.0, 60.1, 56.4, 56.3, 31.2, 20.8, 19.3, 14.0. **ESI-MS** (HR): *m/z* $[M+H]^+$ calcd for $C_{30}H_{29}N_2O_6$: 513.2020, found: 513.2045; *m/z* $[M+Na]^+$ calcd for $C_{30}H_{28}N_2NaO_6$: 535.1840, found: 535.1823.

4.3.9. (E)-4-(6-(4-dodecyloxy-3-methoxystyryl)-4-(dicyanomethylene)-4H-pyran-2-yl)-2-methoxy phenylacetate, 5c

To a stirred solution of (*E*)-2-(4-dodecyloxy-3-methoxystyryl)-6-(4-hydroxy-3-methoxyphenyl)-4H-pyran-4-one **4c** (1.30 g, 2.43 mmol) in Ac_2O (100 mL) at room temperature was added malononitrile (900 mg, 13.62 mmol, 5.60 eq.) and the mixture was refluxed at 140 °C during 3 h (CCM, SiO_2, DCM 100 %). The reaction mixture was cooled to room temperature and then quenched with water (100 mL). Under stirring conditions, Na_2CO_3 (1 M) was added to the mixture in batches and the pH value of the mixture was adjusted to 7. The crude product was extracted with DCM and the organic phase was separated. The aqueous phase was further extracted with DCM (4 × 50 mL). The combined organic phase was washed with water (3 × 50 mL) and brine (3 × 50 mL) then dried over Na_2SO_4, filtered, and evaporated under reduced pressure. Chromatography on silica gel with DCM 100 % afforded the title compound **5c** as an orange solid (1.46 mg, 96 %). ***Rf***: 0.32 (DCM 100 %). **M.p.**: 162 °C. **IR** (ATR, cm^{-1}): 2918, 2210, 1759, 1643, 1589, 1553, 1499. **UV–vis** (DMSO): 407 nm. **^{1}H NMR** (400 MHz, $CDCl_3$): δ 7.50 (dd, $J_{H,H}$ = 8.3, 2.1 Hz, 1H; Ar-*H*), 7.45 (d, $J_{H,H}$ = 15.9 Hz, 1H; $H_{ethyl\ \beta}$), 7.36 (d, $J_{H,H}$ = 2.0 Hz, 1H; Ar-*H*), 7.23 (d, $J_{H,H}$ = 8.3 Hz, 1H; Ar-*H*), 7.11 (dd, $J_{H,H}$ = 8.4, 2.0 Hz, 1H; Ar-*H*), 7.08 (d, $J_{H,H}$ = 1.9 Hz, 1H; Ar-*H*), 7.03 (d, $J_{H,H}$ = 2.0 Hz, 1H; H_{pyrone}), 6.90 (d, $J_{H,H}$ = 8.3 Hz, 1H; Ar-*H*), 6.76 (d, $J_{H,H}$ = 2.0 Hz, 1H; H_{pyrone}), 6.66 (d, $J_{H,H}$ = 15.9 Hz, 1H; $H_{ethyl\ \alpha}$), 4.07 (t, $J_{H,H}$ = 6.9 Hz, 2H; OCH_2), 3.96 (s, 3H; OCH_3), 3.95 (s, 3H; OCH_3), 2.36 (s, 3H; $OC(O)CH_3$), 1.87 (m, 2H; OCH_2CH_2), 1.45 (m, 2H; $OCH_2CH_2CH_2$), 1.38–1.27 (m, 16H; $(CH_2)_n$), 0.88 (t, $J_{H,H}$ = 6.8 Hz, 3H; CH_2CH_3). **^{13}C {^{1}H} NMR** (100 MHz, $CDCl_3$): δ 165.7, 159.3, 159.2, 156.1, 152.1, 151.5, 150.0, 143.3, 138.6, 129.5, 127.4, 124.0, 122.9, 119.6, 116.0, 115.4, 115.3, 112.7, 110.2, 109.9, 107.0, 104.4, 69.3, 60.2, 56.4, 56.3, 32.1, 29.80, 29.78, 29.74, 29.69, 29.52, 29.49, 29.2, 26.1, 22.8, 20.8, 14.3. **ESI-MS** (HR): *m/z* $[M+H]^+$ calcd for $C_{38}H_{45}N_2O_6$: 625.3272, found: 625.3238; *m/z* $[M+Na]^+$ calcd for $C_{38}H_{44}N_2NaO_6$: 647.3092, found: 647.3040.

4.3.10. (E)-4-(4-(dicyanomethylene)-6-(4-(dimethylamino)-3-methoxystyryl)-4H-pyran-2-yl)-2-methoxyphenylacetate, 5d

To a stirred solution of (*E*)-2-(4-(dimethylamino)-3-methoxystyryl)-6-(4-hydroxy-3-methoxy phenyl)-4H-pyran-4-one **4d** (65 mg, 0.17 mmol) in Ac_2O (10 mL) at room temperature was added malononitrile (55 mg, 0.83 mmol, 5.05 eq.) and the mixture was refluxed at 140 °C during 3 h (CCM, SiO_2, Cyclohexane/EtOAc 3:2). The reaction mixture was cooled to room temperature and then quenched with water (20 mL). Under stirring conditions, Na_2CO_3 (1 M) was added to the mixture in batches and the pH value of the mixture was adjusted to 7. The crude product was extracted with DCM and the organic phase was separated. The aqueous phase was further extracted with DCM (4 × 10 mL). The combined organic phase was washed with water (3 × 10 mL) and brine (3 × 10 mL) then dried over Na_2SO_4, filtered, and evaporated under reduced pressure. Chromatography on silica gel with Cyclohexane/EtOAc 3:2 afforded the title compound **5d** as a red solid (43 mg, 54 %). ***Rf***: 0.28 (Cyclohexane/EtOAc 3:2). **M.p.**: 232 °C. **IR** (ATR, cm^{-1}): 2970, 2901, 2201, 1769, 1636, 1587, 1543, 1489. **UV–vis** (DMSO): 418 nm. **^{1}H NMR** (400 MHz, $CDCl_3$): δ 7.50 (dd, $J_{H,H}$ = 8.3, 2.0 Hz, 1H; Ar-*H*), 7.46 (d, $J_{H,H}$ = 15.9 Hz, 1H; $H_{ethyl\ \beta}$), 7.36 (d, $J_{H,H}$ = 1.9 Hz, 1H; Ar-*H*), 7.23 (d, $J_{H,H}$ = 8.3 Hz, 1H; Ar-*H*), 7.11 (dd, $J_{H,H}$ = 8.4, 2.0 Hz, 1H; Ar-*H*), 7.04 (d, $J_{H,H}$ = 2.0 Hz, 1H; Ar-*H*), 7.03 (d, $J_{H,H}$ = 2.0 Hz, 1H; H_{pyrone}), 6.93 (m, 1H; Ar-*H*), 6.76 (d, $J_{H,H}$ = 1.9 Hz, 1H; H_{pyrone}), 6.66 (d, $J_{H,H}$ = 15.9 Hz, 1H; $H_{ethyl\ \alpha}$), 3.97 (s, 3H; OCH_3), 3.96 (s, 3H; OCH_3), 2.92 (s, 6H; $N(CH_3)_2$), 2.37 (s, 3H; $OC(O)CH_3$). **^{13}C{^{1}H} NMR** (100 MHz, $CDCl_3$): δ 165.6, 159.3, 156.0, 152.1, 143.9, 143.3, 138.5, 129.5, 127.9, 124.1, 122.8, 119.6, 117.9, 115.4, 115.3, 110.2, 109.7, 107.0, 104.4, 56.4, 55.9, 43.2, 20.8. **ESI-MS** (HR): *m/z* $[M+H]^+$ calcd for $C_{28}H_{26}N_3O_5$: 484.1867, found: 484.1897; *m/z* $[M+Na]^+$ calcd for $C_{28}H_{25}N_3NaO_5$: 506.1686, found: 506.1734.

4.3.11. (E)-2-(2-(4-hydroxy-3-methoxyphenyl)-6-(4-hydroxy-3-methoxystyryl)-4H-pyran-4-ylidene) malononitrile, 6a

To a stirred solution of (*E*)-4-(2-(6-(4-acetoxy-3-methoxyphenyl)-4-(dicyanomethylene)-4H-pyran-2-yl)vinyl)-2-methoxyphenyl acetate **5a** (17 mg, 34.1 μmol) in MeOH (5 mL) at room temperature was added an excess of K_2CO_3 (47 mg, 0.34 mmol, 10 eq.) and the mixture was refluxed at 65 °C during 2 h (CCM, SiO_2, Cyclohexane/EtOAc 1:1). The reaction mixture was cooled to room temperature and then quenched with water (10 mL). Under stirring conditions, HCl (1 M) was added to the mixture in batches and the pH value of the mixture was adjusted to 7. The crude product was extracted with DCM and the organic phase was separated. The aqueous phase was further extracted with DCM (4 × 10 mL). The combined organic phase was washed with water (3 × 10 mL) and brine (3 × 10 mL) then dried over Na_2SO_4, filtered, and evaporated under reduced pressure. Chromatography on silica gel with Cyclohexane/EtOAc 1:1 afforded the title compound **6a** as a brown solid (14 mg, 99 %). ***Rf***: 0.32 (Cyclohexane/EtOAc 1:1). **M.p.**: 265 °C. **IR** (ATR, cm^{-1}): 3219, 2970, 2901, 2212, 1636, 1589, 1541, 1506. **^{1}H NMR** (400 MHz, DMSO-d_6): δ 10.12 (s, 1H; O*H*), 9.68 (s, 1H; O*H*), 7.62 (dd, $J_{H,H}$ = 8.4, 2.1 Hz, 1H; Ar-*H*), 7.58 (d, $J_{H,H}$ = 16.0 Hz, 1H; $H_{ethyl\ \beta}$), 7.52 (d, $J_{H,H}$ = 2.0 Hz, 1H; Ar-*H*), 7.40 (d, $J_{H,H}$ = 1.5 Hz, 1H; Ar-*H*), 7.25 (d, $J_{H,H}$ = 16.0 Hz, 1H; $H_{ethyl\ \alpha}$), 7.19 (dd, $J_{H,H}$ = 8.2, 1.5 Hz, 1H; Ar-*H*), 7.02 (d, $J_{H,H}$ = 1.9 Hz, 1H; H_{pyrone}), 6.99 (d, $J_{H,H}$ = 8.4 Hz, 1H; Ar-*H*), 6.84 (d, $J_{H,H}$ = 8.4 Hz, 1H; Ar-*H*), 6.83 (d, $J_{H,H}$ = 1.9 Hz, 1H; H_{pyrone}), 3.93 (s, 3H; OCH_3), 3.85 (s, 3H; OCH_3). **^{13}C{^{1}H} NMR** (100 MHz, DMSO-d_6): δ 160.1, 159.7, 156.2, 151.2, 149.4, 148.12, 148.07, 138.3, 126.6, 123.5, 121.0, 120.7, 115.8, 116.1, 115.8, 115.6, 110.6, 110.2, 106.0, 101.5, 55.9, 55.7, 55.1. **ESI-MS** (HR): *m/z* $[M+H]^+$ calcd for $C_{24}H_{19}N_2O_5$: 415.1288, found: 415.1306; *m/z* $[M+Na]^+$ calcd for $C_{24}H_{19}N_2NaO_5$: 437.1108, found: 437.1070.

4.3.12. (E)-2-(2-(4-butoxy-3-methoxystyryl)-6-(4-hydroxy-3-methoxyphenyl)-4H-pyran-4-ylidene) malononitrile, 6b

To a stirred solution of (*E*)-4-(6-(4-butoxy-3-methoxystyryl)-4-(dicyanomethylene)-4H-pyran-2-yl)-2-methoxyphenyl acetate **5b** (1.40 g, 2.24 mmol) in MeOH (100 mL) at room temperature was added an excess of K_2CO_3 (1.50 g, 10.85 mmol, 4.84 eq.) and the mixture was refluxed at 65 °C during 2 h (CCM, SiO_2, DCM 100 %). The reaction mixture was cooled to room temperature and then quenched with water (10 mL). Under stirring conditions, HCl (1 M) was added to the mixture in batches and the pH value of the mixture was adjusted to 7. The crude product was extracted with DCM and the organic phase was separated. The aqueous phase was further extracted with DCM (4 × 50 mL). The combined organic phase was washed with water (3 × 50 mL) and brine (3 × 50 mL) then dried over Na_2SO_4, filtered, and evaporated under reduced pressure. Chromatography on silica gel with DCM 100 % afforded the title compound **6b** as a brown solid (85.4 mg, 98 %). ***Rf***: 0.35 (DCM 100 %). **M.p.**: 196 °C. **IR** (ATR, cm^{-1}): 2970, 2901, 2208, 1645, 1593, 1514, 1506. **^{1}H NMR** (400 MHz, DMSO-d_6): δ 10.10 (s, 1H; O*H*), 7.63 (dd, $J_{H,H}$ = 8.4, 2.0 Hz, 1H; Ar-*H*), 7.60 (d, $J_{H,H}$ = 15.9 Hz, 1H; $H_{ethyl\ \beta}$), 7.52 (d, $J_{H,H}$ = 2.2 Hz, 1H; Ar-*H*), 7.41 (d, $J_{H,H}$ = 1.9 Hz, 1H; Ar-*H*), 7.31 (d, $J_{H,H}$ = 16.1 Hz, 1H; $H_{ethyl\ \alpha}$), 7.29 (dd, $J_{H,H}$ = 8.4, 2.0 Hz, 1H; Ar-*H*), 7.03 (d, $J_{H,H}$ = 2.0 Hz, 1H; H_{pyrone}), 7.02 (d, $J_{H,H}$ = 8.4 Hz, 1H; Ar-*H*), 6.99 (d, $J_{H,H}$ = 8.4 Hz, 1H; Ar-*H*), 6.86 (d, $J_{H,H}$ = 2.0 Hz, 1H; H_{pyrone}), 4.02 (t, $J_{H,H}$ = 6.5 Hz, 2H; OCH_2CH_2), 3.93 (s, 3H; OCH_3), 3.84 (s, 3H; OCH_3), 1.72 (m, 2H; $OCH_2CH_2CH_2$), 1.44 (m, 2H; CH_2CH_3), 0.94 (t, $J_{H,H}$ = 7.4 Hz, 3H; CH_2CH_3). **^{13}C{^{1}H} NMR** (100 MHz, DMSO-d_6): δ 160.1, 159.5, 156.2, 151.2, 150.4, 149.0, 148.1, 137.8, 127.7, 123.1, 121.0, 120.7, 116.7, 116.1, 116.0, 115.7, 112.6, 110.2, 110.0, 106.3, 101.6, 67.9, 55.9, 55.6, 55.4, 30.7, 18.7, 13.7. **ESI-MS** (HR): *m/z* $[M+H]^+$ calcd for $C_{28}H_{27}N_2O_5$: 471.1914, found: 471.1959; *m/z* $[M+Na]^+$ calcd for $C_{28}H_{26}N_2NaO_5$: 493.1734, found: 493.1691.

4.3.13. (E)-2-(2-(4-dodecyloxy-3-methoxystyryl)-6-(4-hydroxy-3-methoxyphenyl)-4H-pyran-4-ylidene) malononitrile, 6c

To a stirred solution of (*E*)-4-(6-(4-dodecyloxy-3-methoxystyryl)-4-

(dicyanomethylene)-4H-pyran-2-yl)-2-methoxyphenyl acetate **5c** (1.40 g, 2.24 mmol) in MeOH (100 mL) at room temperature was added an excess of K_2CO_3 (1.50 mg, 10.85 mmol, 4.84 eq.) and the mixture was refluxed at 65 °C during 2 h (CCM, SiO_2, DCM 100 %). The reaction mixture was cooled to room temperature and then quenched with water (50 mL). Under stirring conditions, HCl (1 M) was added to the mixture in batches and the pH value of the mixture was adjusted to 7. The crude product was extracted with DCM and the organic phase was separated. The aqueous phase was further extracted with DCM (4x50 mL). The combined organic phase was washed with water (3x50 mL) and brine (3x50 mL) then dried over Na_2SO_4, filtered, and evaporated under reduced pressure. Chromatography on silica gel with DCM 100 % afforded the title compound **6c** as an orange solid (1.28 g, 98 %). ***R_f***: 0.28 (DCM 100 %). **M.p.**: 146 °C. **IR** (ATR, cm^{-1}): 3223, 2916, 2849, 2201, 1645, 1591, 1514, 1499. **^{1}H NMR** (400 MHz, $CDCl_3$): δ 7.50 (dd, $J_{H,H}$ = 8.4, 2.1 Hz, 1H; Ar-*H*), 7.45 (d, $J_{H,H}$ = 15.9 Hz, 1H; $H_{ethyl\ \beta}$), 7.27 (d, $J_{H,H}$ = 2.1 Hz, 1H; Ar-*H*), 7.11 (dd, $J_{H,H}$ = 8.4, 2.0 Hz, 1H; Ar-*H*), 7.08 (d, $J_{H,H}$ = 8.4 Hz, 1H; Ar-*H*), 7.07 (d, $J_{H,H}$ = 1.9 Hz, 1H; Ar-*H*), 6.97 (d, $J_{H,H}$ = 2.0 Hz, 1H; H_{pyrone}), 6.90 (d, $J_{H,H}$ = 8.3 Hz, 1H; Ar-*H*), 6.73 (d, $J_{H,H}$ = 1.9 Hz, 1H; H_{pyrone}), 6.65 (d, $J_{H,H}$ = 15.9 Hz, 1H; $H_{ethyl\ \alpha}$), 6.09 (br s, 1H; O*H*), 4.07 (t, $J_{H,H}$ = 6.9 Hz, 2H; OCH_2), 4.03 (s, 3H; OCH_3), 3.95 (s, 3H; OCH_3), 1.87 (m, 2H; OCH_2CH_2), 1.47 (m, 2H; $OCH_2CH_2CH_2$), 1.36–1.27 (m, 16H; $(CH_2)_n$), 0.88 (t, $J_{H,H}$ = 6.8 Hz, 3H; CH_2CH_3). **^{13}C {^{1}H} NMR** (100 MHz, $CDCl_3$): δ 160.0, 159.0, 156.3, 151.4, 150.0, 149.9, 147.2, 138.2, 127.5, 122.8, 122.7, 121.0, 116.2, 115.8, 115.7, 115.4, 112.7, 109.8, 108.3, 106.8, 102.8, 69.3, 58.9, 56.5, 56.3, 32.1, 29.80, 29.78, 29.73, 29.69, 29.52, 29.49, 29.2, 26.1, 22.8, 14.3. **ESI-MS** (HR): *m/z* $[M+H]^+$ calcd for $C_{36}H_{43}N_2O_5$: 583.3166, found: 583.3157; *m/z* $[M+Na]^+$ calcd for $C_{36}H_{42}N_2NaO_5$: 605.2986, found: 605.2967.

4.3.14. *(E)-2-(2-(4-(dimethylamino)-3-methoxystyryl)-6-(4-hydroxy-3-methoxyphenyl)-4H-pyran-4-ylidene)malononitrile,* ***6d***

To a stirred solution of (*E*)-4-(4-(dicyanomethylene)-6-(4-(dimethylamino)-3-methoxystyryl)-4H-pyran-2-yl)-2-methoxyphenyl acetate **5d** (40 mg, 82.7 μmol) in MeOH (5 mL) at room temperature was added an excess of K_2CO_3 (40 mg, 0.29 mmol, 3.50 eq.) and the mixture was refluxed at 65 °C during 1 h (CCM, SiO_2, Cyclohexane/EtOAc 1:1). The reaction mixture was cooled to room temperature and then quenched with water (10 mL). Under stirring conditions, HCl (1 M) was added to the mixture in batches and the pH value of the mixture was adjusted to 7. The crude product was extracted with DCM and the organic phase was separated. The aqueous phase was further extracted with DCM (4x10 mL). The combined organic phase was washed with water (3x10 mL) and brine (3x10 mL) then dried over Na_2SO_4, filtered, and evaporated under reduced pressure. Chromatography on silica gel with Cyclohexane/EtOAc 1:1 afforded the title compound **6d** as a dark red solid (35.7 mg, 98 %). ***R_f***: 0.32 (Cyclohexane/EtOAc 1:1). **M.p.**: 225 °C. **IR** (ATR, cm^{-1}): 2988, 2901, 2208, 1636, 1589, 1520, 1422. **^{1}H NMR** (400 MHz, DMSO-d_6): δ 10.10 (s, 1H; O*H*), 7.62 (dd, $J_{H,H}$ = 8.4, 2.1 Hz, 1H; Ar-*H*), 7.59 (d, $J_{H,H}$ = 15.8 Hz, 1H; $H_{ethyl\ \beta}$), 7.51 (d, $J_{H,H}$ = 2.2 Hz, 1H; Ar-*H*), 7.35 (d, $J_{H,H}$ = 1.7 Hz, 1H; Ar-*H*), 7.27 (d, $J_{H,H}$ = 16.0 Hz, 1H; $H_{ethyl\ \alpha}$), 7.24 (dd, $J_{H,H}$ = 8.2, 1.7 Hz, 1H; Ar-*H*), 7.02 (d, $J_{H,H}$ = 2.0 Hz, 1H; H_{pyrone}), 6.99 (d, $J_{H,H}$ = 8.4 Hz, 1H; Ar-*H*), 6.87 (d, $J_{H,H}$ = 8.3 Hz, 1H; Ar-*H*), 6.84 (d, $J_{H,H}$ = 2.0 Hz, 1H; H_{pyrone}), 3.93 (s, 3H; OCH_3), 3.87 (s, 3H; OCH_3), 2.82 (s, 6H; $N(CH_3)_2$). **^{13}C{^{1}H} NMR** (100 MHz, DMSO-d_6): δ 160.1, 159.7, 156.1, 151.3, 151.2, 148.1, 144.2, 138.0, 127.8, 123.2, 121.0, 120.8, 117.0, 116.1, 116.0, 115.9, 115.8, 110.2, 106.1, 101.5, 55.9, 55.6, 55.1, 42.3. **ESI-MS** (HR): *m/z* $[M+H]^+$ calcd for $C_{26}H_{24}N_3O_4$: 442.1761, found: 442.1792; *m/z* $[M+Na]^+$ calcd for $C_{26}H_{23}N_3NaO_4$: 464.1581, found: 464.1554.

4.4. *Absorption and emission spectra*

UV – visible spectra were recorded on a PerkinElmer Lambda 1050 UV – Vis – NIR spectrophotometer using a 1 cm optical path length cell at 25 °C, unless otherwise specified. The steady-state measurements were recorded on a Jobin Yvon Fluorolog-3 spectrofluorometer from Horiba Scientific and the FluorEssence program. The excitation source was a 450 W xenon lamp, and the detector used was R-928 operating at a voltage of 950 V. Excitation and emission slits width were 1 nm. The fluorescence quantum yields were determined using quinine sulphate and tris(bipyridine)ruthenium (II) chloride as the standard (Φ = 0.53 in H_2SO_4, 0.05 M and Φ = 0.028 in H_2O, respectively) using

$$\Phi_x = \Phi_s\left(\frac{Grad_x}{Grad_s}\right)\left(\frac{\eta_x^2}{\eta_s^2}\right)$$

where φ, Grad, and η represent the fluorescence quantum yield, gradient from the plot of integrated fluorescence intensity versus absorbance, and refractive index of the solvent, respectively. The subscripts S and X denote the standard and test, respectively.

4.5. *Kinetics and fatigue resistance*

The photoisomerization was carried out on a 1.0 cm path length quartz cell placed on a foursided cuvette holder (Cuvette Holder with Four Light Ports, CVH100 Thorlabs). Unless otherwise specified, the concentration of the samples was 40 μM. The kinetics of the photoisomerization process were measured by following the absorption spectrum during irradiation by selected LEDs, placed perpendicular to the absorbance measurement. To reach the PSS of the $E \rightarrow Z$ isomerization, the *E*-stereoisomer was illuminated within the π-π* band using an M375L4.1540 mW LED (LED Power Output 1540 mW, 2 % power used) with a central wavelength of 375 nm and a bandwidth (FWHM) of 9 nm. For the reverse transformation, $Z \rightarrow E$ isomerization, the compound was excited within the n-π* band using an M300L4.32 mW LED (LED Power Output: 47 mW, full power used) with a central wavelength of 300 nm and a bandwidth (FWHM) of 20 nm. The thermal return process between *Z* and *E* isomers was analyzed by measuring the changes of the maximum absorbance wavelength at 25 and 40 °C, respectively. Kinetic monitoring of absorbance was performed using an Ocean Optics USB2000 + XR CCD sensor and kinetic constants were determined using "Biokine" software.

4.6. *Determination of the photoisomerization quantum yield by UV–vis spectroscopy*

The equipment used and the protocol followed are the same as those described in section 4.5.

Since the thermal back-switch is very slow in all solvents, it was considered negligible on the time scale of the photokinetic measurements. The overall differential photokinetic equation relating the concentration variation of each isomer as a function of time and the photoisomerization quantum yields can therefore be written:

$$\frac{dC_Z}{dt} = -\frac{dC_E}{dt} = \Phi_{EZ} \bullet I_E^{abs}(\lambda_{irr},\ t) - \Phi_{ZE} \bullet I_Z^{abs}(\lambda_{abs},\ t) \quad (1)$$

where Φ_{EZ} is the $E \rightarrow Z$ photoisomerization quantum yield, Φ_{ZE} is the $Z \rightarrow E$ photoisomerization quantum yield and I^{abs} is the time-dependent intensity absorbed by the compound at the irradiation wavelength λ_{irr}:

$$I_E^{abs}(\lambda_{abs}, t) = \left[\frac{1 - 10^{-Abs(\lambda_{irr},t)}}{Abs(\lambda_{irr}, t)}\right] \bullet I_0(\lambda_{irr}) \bullet \varepsilon_E(\lambda_{irr}) \bullet l \bullet C_E(t) \quad (2)$$

$$I_Z^{abs}(\lambda_{abs}, t) = \left[\frac{1 - 10^{-Abs(\lambda_{irr},t)}}{Abs(\lambda_{irr}, t)}\right] \bullet I_0(\lambda_{irr}) \bullet \varepsilon_Z(\lambda_{irr}) \bullet l \bullet C_Z(t) \quad (3)$$

with $Abs(\lambda_{irr},t)$, the absorbance at the irradiation wavelength during the time of the experiment, *l*, the path length and $I_0(\lambda_{irr})$, the incident irradiation intensity. By setting at a low $E \rightarrow Z$ conversion level, the impact and effect of $Z \rightarrow E$ photoisomerization can be neglected, and thus equation (1) can be simplified to equation (4):

$$\frac{dC_Z}{dt} = -\frac{dC_E}{dt} \approx I_0(\lambda_{irr}) \bullet \Phi_{EZ} \bullet \left(1 - 10^{-\varepsilon_E l C_E(t)}\right) \quad (4)$$

The absorbed light intensity $I^{abs}(\lambda_{irr})$ during $E \rightarrow Z$ and $Z \rightarrow E$ isomerization at the corresponding irradiation wavelengths and initial concentration C_{E0} of the *E*-isomer was determined using Eq. (5). The value obtained was similar to that resulting from the use of a Thorlabs PM16-140 - USB Power Meter (Integrating Sphere Sensor, FC Fiber Adapter, Si, 350–1100 nm, 500 mW Max):

$$I^{abs}(\lambda_{irr}) = I_0(\lambda_{irr}) - I_T(\lambda_{irr}) \quad (5)$$

where $I_T(\lambda_{irr})$ is the intensity of the transmitted unabsorbed light. Under the conditions of the experiment, the $I_T(\lambda_{irr})$ term can be neglected as the irradiation power is low (2 % of the 375 nm LED maximal power). In order to determine $I_0(\lambda_{irr})$ at 375 nm with equation (5), *o*-nitrobenzaldehyde was used as a reference and chemical actinometer. Indeed, *o*-nitrobenzaldehyde is transformed into o-nitrobenzoic acid under irradiation at 405 nm.

$$I_{0\,405\,o-NB} = \frac{k}{2.303\varepsilon_{o-NB\,405}\Phi_{0-NB\,405}l} \quad (6)$$

where: $\varepsilon_{o\text{-NB}\ 405}$ is the molar extinction coefficient of *o*-nitrobenzaldehyde at the irradiation wavelength (405 nm), $\Phi_{o\text{-NB}\ 405}$ is the quantum yield of the photodegradation of *o*-nitrobenzaldehyde at the irradiation wavelength, *l* is the path length, and *k* is the first-order photodegradation slope of *o*-nitrobenzaldehyde plotted under low-light-absorbing conditions:

$$\ln\left(\frac{[o-nitrobenzaldehyde]_t}{[o-nitrobenzaldehyde]_0}\right) = -kt \quad (7)$$

Then, the incident light intensity $I_0(\lambda_{irr})$ at 375 nm was determined using Eq. (8): [62]

$$I_0(\lambda_{irr}) = I_{0405o-NB} \bullet \frac{(I_0(\lambda_{irr}))_W}{(I_{0405})_W} \bullet \frac{E_{photon405}}{E_{photon\lambda_{irr}}} \quad (8)$$

where $E_{photon\lambda_{irr}}$ is the energy of a photon at the corresponding irradiation wavelength. Furthermore, $I_0(\lambda_{irr})$ and $I_{0405o-NB}$ are expressed in μeinstein•L^{-1}•s^{-1} while $(I_0(\lambda_{irr}))_W$ and $(I_{0405})_W$ are in watts.The incident absorbed light intensity $I_a(\lambda_{irr})$ was estimated to be 6 μeinstein•L^{-1}•s^{-1} under the irradiation conditions of the experiments. Finally, the photoisomerization quantum yields Φ_{EZ} of the compounds **4a-d** in the four solvents could be determined by solving the equation (4). The backward photoisomerization quantum yields Φ_{ZE} were determined at PSS, where the concentration of each isomer is stationary. This fact combined with the negligible impact of the thermal contribution allows to use the previous equations approximating the concentration of each isomer at PSS by the ratio of the product of the photoisomerization quantum yield and the molar extinction coefficient (Eq. (9)).

$$\frac{C_{Z,PSS}}{C_{E,PSS}} \approx \frac{\Phi_{EZ}\varepsilon_{E,\lambda}}{\Phi_{ZE}\varepsilon_{Z,\lambda}} \quad (9)$$

4.7. Determination of the photoisomerization quantum yield by in-situ NMR measurements

In order to verify and validate the UV–vis approach described in 5.6 for the measurement of Φ_{EZ} the $E \rightarrow Z$ photoisomerization quantum yields, we used an independent approach based on NMR measurements of compounds **4a** and **4d** in DMSO-d_6 under *in-situ* light irradiation. The procedure used here is described by Ji *et al.*, [63] and relies on equation (4) where the concentration of the starting *E*-isomer is chosen high enough to simplify the equation down to Eq. (10):

$$-\frac{dC_E}{dt} \approx I_a(\lambda_{irr}) \text{ x } \Phi_{EZ} \quad (10)$$

The procedure therefore consists in three steps: First the incident light intensity in the NMR tube $I_0(\lambda_{irr})$ has to be determined at the irradiation wavelength (375 nm); then the minimum concentration of the starting photo-isomer has to be determined in order for the expression to be independent from isomer concentration; finally, the zeroth order kinetic constant $k_0 = -\frac{dC}{dt}$ (mol•L^{-1}•s^{-1}) corresponding to the concentration variation of the photo-isomers can be measured in order to calculate the photoisomerization quantum yield from equation (10).

The light intensity received by the sample was measured before and after the kinetic measurements on compounds **4a** and **4b** according to the procedure described in ref [63]. We measured the zeroth-order kinetic constant k_0 of the *o*-nitrobenzaldehyde photoreaction in $CDCl_3$ (C = 90 mM) by acquiring one spectrum every 15 s during the first 4 min of illumination and inferred light intensities of $I_0(375\,nm) = 165.5 \pm 5$ μeinstein•L^{-1}•s^{-1} for the 375 nm LED (full power I = 1200 mA). The error margin was estimated based on the difference in the light intensity measured before and after the kinetic measurements on the photo-isomer samples.

The minimum concentration of the starting photo-isomers for the validity of equation (10) was determined based on a series of kinetic measurements on compound **4a** for increasing photo-isomer concentration ranging from 5 to 80 mM. By this way a concentration of 60 mM was found sufficient to perform quantum yield measurements on our photoswitches.

The zeroth order kinetic constants measurements of compounds **4a** and **4b** were performed by following the time evolution of the O-CH_3 proton signal integrals (at 3.94 and 3.89 ppm for the *E*-isomer and 3.62 and 3.56 ppm for the *Z*-isomer) by acquiring one spectrum every 30 s during the first 14 min of illumination (375 nm) and performing a linear fit of the time evolution of the O-CH_3 proton signal integrals (Figure S13).

^{1}H NMR monitoring for *in situ* irradiation NMR analysis was performed at T = 293 K on a Bruker Avance III HD 300 MHz spectrometer equipped with a 5 mm BBO probe head. All NMR data were processed using TopSpin (Bruker) software. The kinetic analysis was performed by customized "pseudo 2D" experiments synchronized with the LED illumination by the inclusion of TTL commands allowing the NMR spectrometer to trigger the irradiation. The NMR measurements were acquired with a 30° excitation pulse, an accumulation over eight scans, and an interscan delay of 2.74 s.

As in our earlier studies, [41,64] *in situ* sample irradiation was performed using a setup inspired by the work of Feldmeier *et al.*, [65] by directly coupling the 375 nm LED to a 1000 μm multimode optical fiber. At the tip of the fiber, the jacket was removed, and the fiber was sandblasted over the length of the detection NMR coil to allow homogeneous radial irradiation of the sample. The fiber was then inserted into a coaxial insert glasstube filled with D_2O. This coaxial tube was then inserted in the 5 mm NMR tube containing the samples.

4.8. Determination of Z-isomer absorption spectra and molar absorption coefficient

The equipment used and the protocol followed are the same as those described in section 4.5.

Similarly to a recent study, [64] by combining the UV–vis spectrum of each *E*-isomer in each solvent at GS and PSS and the rate of *Z*-isomer formed at PSS1 measured by NMR, the absorption spectrum of *Z*-isomers could be obtained according to equation (11): [47]

$$A_Z(\lambda) = A_E(\lambda) + \frac{A_{PSS}(\lambda) - A_E(\lambda)}{\alpha_Z} \quad (11)$$

It is nevertheless important to point out here that the use of *in-situ* irradiation in both NMR and UV/vis experiments allows direct photoisomerization monitoring; this is essential to obtain the quantitative results presented here since any degradation of the photo-isomers

during the irradiation can be detected.

4.9. Photothermal measurements

In order to characterize the photothermal conversion efficiency η, 200 μL of a solution of each compound **6a-d** is placed in 96-well plate at different concentrations (5/10/20/40 μM) in DMSO. The absorption of these samples was previously measured with a microplates SAFAS Xeniux XML. The irradiation and photothermal measurement setup are a home-made setup composed of a continuous-wave 470 nm blue diode MDL-F-470 laser (2 W) connected to a 400 μm fiber of CNILasers (Full Name) whose power is modulated by a controller. The thermal camera is a Xi400 camera from Optris (IR camera Optris Xi 400 "spot finder" compact: 382 × 288 Pixel / 80 Hz, Objective: 18° x 14° objectiv / f = 20 mm). Finally, the protective enclosure is made with components from Thorlabs.

Using this setup, the solutions were irradiated with the 470 nm laser for 400 s with an irradiance of 0.68 $W.cm^{-2}$. After extinction of the laser, a return to natural room temperature comes after 800 s. The temperature of the solution is recorded with a digital thermometer with an accuracy of 0.1 °C every 0.5 s. The photothermal conversion efficiency was calculated following the method reported by Roper. The resistance to photothermal fatigue is studied by performing 5 cycles as described above (irradiation then return to room temperature) with an absorption measurement between each cycle.

4.10. Determination of the photothermal conversion efficiency

The photothermal conversion efficiency (η) was calculated as previously reported. [66–67] Briefly, η was determined by using the following equation (12):

$$\eta = \frac{hS(T_{Max} - T_{Surr}) - Q_{Dis}}{I\left(1 - 10^{-A_{470}}\right)} \tag{12}$$

where h is the heat transfer coefficient, and S (0.36 cm^2) is the surface area of the container. $T_{Max} - T_{Surr}$ is the temperature change of the **6a-d** solution at the maximum steady-environmental temperature, I (0.245 W) is the power of the laser irradiating the surface area of the container, A_{470} is the absorbance of **6a-d** solutions at 470 nm, and Q_{Dis} is the heat dissipation from light absorbed by the DMSO and the container. The Q_{Dis} (3.2 mW) was measured independently using the same method containing DMSO without organic compounds.

The value of hS is derived according to the equation (13):

$$\tau_s = \frac{m_{DMSO} C_{DMSO}}{hS} \tag{13}$$

where m_{DMSO} and C_{DMSO} are the mass (0.22 g) and heat molar capacity (1912 $J \bullet °C^{-1} \bullet kg^{-1}$) of DMSO used as solvent, respectively. τ_s, the time constant for heat transfer from the system, is obtained by drawing linear time data from the cooling period time against ln(θ). ln(θ), defined as the ratio of ΔT to ΔT_{max}, was calculated from the following equation (14):

$$\ln(\theta) = \frac{(T - T_{min})}{\Delta T_{max}} \tag{14}$$

CRediT authorship contribution statement

Jérémy Pecourneau: Writing – original draft, Methodology, Investigation, Formal analysis. **Raúl Losantos:** Writing – original draft, Methodology, Investigation, Formal analysis. **Axel Gansmuller:** Writing – original draft, Methodology, Investigation, Formal analysis. **Stéphane Parant:** Methodology. **Yann Bernhard:** Writing – review & editing. **Maxime Mourer:** Writing – review & editing, Supervision, Funding acquisition, Formal analysis, Conceptualization. **Antonio Monari:** Writing – review & editing, Supervision, Formal analysis, Conceptualization. **Andreea Pasc:** Writing – review & editing, Supervision, Project administration, Funding acquisition, Formal analysis, Conceptualization.

Declaration of Competing Interest

The authors declare that they have no known competing financial interests or personal relationships that could have appeared to influence the work reported in this paper.

Acknowledgements

J.P. acknowledges French Ministry of Higher Education, Research and Innovation for his PhD grant. R.L. thanks Universidad de La Rioja and Ministerio de Universidades for his "Margarita Salas" grant. The authors greatly acknowledge the NMR Plateforme of Jean Barriol Institut, MassLor Spectrometry and PhotoNS Plateformes of the University of Lorraine. The authors thank F. Dupire for performing mass spectrometry measurements. The authors gratefully acknowledge the University of Lorraine, CNRS, and the European Regional Development Funds (Programme opérationnel FEDER-FSE Lorraine et Massif des Vosges 2014-2020/"Fire Light" project: "Photo-bio-active molecules and nanoparticles") for financial support. All the calculations have been performed on the regional Explor computing center under the project "Dancing under the light". A.M. also thanks ANR and CGI for their financial support of this work through Labex SEAM ANR 11 LABX 086, ANR 11 IDEX 05 02. The support of the IdEx "Université Paris 2019" ANR-18-IDEX-0001 and of the Platform P3MB is gratefully acknowledged.

Appendix A. Supplementary data

Supplementary data to this article can be found online at https://doi.org/10.1016/j.jphotochem.2023.114583.

References

[1] L. Yin, J.-J. Duan, X.-W. Bian, S. Yu, Triple-negative breast cancer molecular subtyping and treatment progress, Breast Cancer Res. 22 (1) (2020) 61, https://doi.org/10.1186/s13058-020-01296-5.
[2] A. McGuigan, P. Kelly, R.C. Turkington, C. Jones, H.G. Coleman, R.S. McCain, Pancreatic cancer: a review of clinical diagnosis, epidemiology, treatment and outcomes, *World J. Gastroenterol.*, 24 (43) (2018) 4846–4861, https://doi.org/10.3748/wjg.v24.i43.4846.
[3] P. Dunkel, J. Ilaš, Targeted cancer therapy using compounds activated by light, Cancers 13 (13) (2021) 3237, https://doi.org/10.3390/cancers13133237.
[4] J. Seung Lee, J. Kim, Y. Ye, T. Kim, Materials and device design for advanced phototherapy systems, Adv. Drug Deliv. Rev. 186 (2022), 114339, https://doi.org/10.1016/j.addr.2022.114339.
[5] J.H. Correia, J.A. Rodrigues, S. Pimenta, T. Dong, Z. Yang, Photodynamic therapy review: principles, photosensitizers, applications, and future directions, Pharmaceutics 13 (9) (2021) 1332, https://doi.org/10.3390/pharmaceutics13091332.
[6] C.A. Robertson, D.H. Evans, H. Abrahamse, Photodynamic therapy (PDT): a short review on cellular mechanisms and cancer research applications for PDT, J. Photochem. Photobiol. B Biol. 96 (1) (2009) 1–8, https://doi.org/10.1016/j.jphotobiol.2009.04.001.
[7] K.H. Nelke, W. Pawlak, J. Leszczyszyn, H. Gerber, Photodynamic therapy in head and neck cancer, Postepy Hig. Med. Dosw. (Online) 68 (2014) 119–128, https://doi.org/10.5604/17322693.1088044.
[8] M. Spitzer, B.A. Krumholz, Photodynamic therapy in gynecology, Obstet. Gynecol. Clin. N. Am. 18 (3) (1991) 649–659, https://doi.org/10.1016/S0889-8545(21)00339-9.
[9] P.C. Mayor, S. Lele, Photodynamic therapy in gynecologic malignancies: a review of the roswell park cancer institute experience, Cancers (Basel) 8 (10) (2016) 88, https://doi.org/10.3390/cancers8100088.
[10] D. Bechet, S.R. Mordon, F. Guillemin, M.A. Barberi-Heyob, Photodynamic therapy of malignant brain tumours: a complementary approach to conventional therapies, Cancer Treat. Rev. 40 (2) (2014) 229–241, https://doi.org/10.1016/j.ctrv.2012.07.004.
[11] M. Kim, H.Y. Jung, H.J. Park, Topical PDT in the treatment of benign skin diseases: principles and new applications, Int. J. Mol. Sci. 16 (10) (2015) 23259–23278, https://doi.org/10.3390/ijms161023259.

[12] D. Gao, R.R. Agayan, H. Xu, M.A. Philbert, R. Kopelman, Nanoparticles for two-photon photodynamic therapy in living cells, Nano Lett 6 (11) (2006) 2383–2386, https://doi.org/10.1021/nl0617179.

[13] *Super-efficient in Vivo Two-Photon Photodynamic Therapy with a Gold Nanocluster as a Type I Photosensitizer | ACS Nano*. https://pubs-acs-org.bases-doc.univ-lorraine.fr/doi/10.1021/acsnano.9b05169 (accessed 2022-10-25).

[14] I. Yakavets, H.-P. Lassalle, I. Yankovsky, F. Ingrosso, A. Monari, L. Bezdetnaya, V. Zorin, Evaluation of temoporfin affinity to β-cyclodextrins assuming self-aggregation, J. Photochem. Photobiol. A Chem. 367 (2018) 13–21, https://doi.org/10.1016/j.jphotochem.2018.07.046.

[15] B. Aslanoglu, I. Yakavets, V. Zorin, H.-P. Lassalle, F. Ingrosso, A. Monari, S. Catak, Optical properties of photodynamic therapy drugs in different environments: the paradigmatic case of temoporfin, Phys. Chem. Chem. Phys. 22 (29) (2020) 16956–16964, https://doi.org/10.1039/D0CP02055A.

[16] M. Girardon, S. Parant, A. Monari, F. Dehez, C. Chipot, E. Rogalska, N. Canilho, A. Pasc, Triggering tautomerization of curcumin by confinement into liposomes, ChemPhotoChem 3 (10) (2019) 1034–1041, https://doi.org/10.1002/cptc.201900159.

[17] G. Gunaydin, M.E. Gedik, S. Ayan, Photodynamic therapy—current limitations and novel approaches, Front. Chem. (2021) 9.

[18] T. Hompland, C.S. Fjeldbo, H. Lyng, Tumor hypoxia as a barrier in cancer therapy: why levels matter, Cancers 13 (3) (2021) 499, https://doi.org/10.3390/cancers13030499.

[19] *The role of hypoxia in the tumor microenvironment and development of cancer stem cell: a novel approach to developing treatment | Cancer Cell International | Full Text*. https://cancerci.biomedcentral.com/articles/10.1186/s12935-020-01719-5 (accessed 2022-10-25).

[20] P. Vaupel, O. Thews, M. Hoeckel, Treatment resistance of solid tumors, Med. Oncol. 18 (4) (2001) 243–259, https://doi.org/10.1385/MO:18:4:243.

[21] D. Kessel, N.L. Oleinick, Cell death pathways associated with photodynamic therapy: an update, Photochem. Photobiol. 94 (2) (2018) 213–218, https://doi.org/10.1111/php.12857.

[22] S. Bonnet, Why develop photoactivated chemotherapy? Dalton Trans. 47 (31) (2018) 10330–10343, https://doi.org/10.1039/C8DT01585F.

[23] S.H.C. Askes, A. Bahreman, S. Bonnet, Activation of a photodissociative ruthenium complex by triplet-triplet annihilation upconversion in liposomes, Angew. Chem. 126 (4) (2014) 1047–1051, https://doi.org/10.1002/ange.201309389.

[24] L.N. Lameijer, D. Ernst, S.L. Hopkins, M.S. Meijer, S.H.C. Askes, S.E. Le Dévédec, S. Bonnet, A red-light-activated ruthenium-caged NAMPT inhibitor remains phototoxic in hypoxic cancer cells, Angew. Chem. 129 (38) (2017) 11707–11711, https://doi.org/10.1002/ange.201703890.

[25] H.S. Han, K.Y. Choi, Advances in nanomaterial-mediated photothermal cancer therapies: toward clinical applications, Biomedicines 9 (3) (2021) 305, https://doi.org/10.3390/biomedicines9030305.

[26] X. Li, J.F. Lovell, J. Yoon, X. Chen, Clinical development and potential of photothermal and photodynamic therapies for cancer, Nat. Rev. Clin. Oncol. 17 (11) (2020) 657–674, https://doi.org/10.1038/s41571-020-0410-2.

[27] Z. Jiang, T. Li, H. Cheng, F. Zhang, X. Yang, S. Wang, J. Zhou, Y. Ding, Nanomedicine potentiates mild photothermal therapy for tumor ablation, Asian J. Pharm. Sci. 16 (6) (2021) 738–761, https://doi.org/10.1016/j.ajps.2021.10.001.

[28] Y. Cai, P. Liang, Q. Tang, X. Yang, W. Si, W. Huang, Q. Zhang, X. Dong, Diketopyrrolopyrrole-triphenylamine organic nanoparticles as multifunctional reagents for photoacoustic imaging-guided photodynamic/photothermal synergistic tumor therapy, ACS Nano 11 (1) (2017) 1054–1063, https://doi.org/10.1021/acsnano.6b07927.

[29] V. Diez-Cabanes, A. Monari, M. Pastore, Competition between the photothermal effect and emission in potential phototherapy agents, J. Phys. Chem. B 125 (31) (2021) 8733–8741, https://doi.org/10.1021/acs.jpcb.1c03977.

[30] J.-S. Ni, X. Zhang, G. Yang, T. Kang, X. Lin, M. Zha, Y. Li, L. Wang, K. Li, A photoinduced nonadiabatic decay-guided molecular motor triggers effective photothermal conversion for cancer therapy, Angew. Chem. Int. Ed. 59 (28) (2020) 11298–11302, https://doi.org/10.1002/anie.202002516.

[31] D. Xi, M. Xiao, J. Cao, L. Zhao, N. Xu, S. Long, J. Fan, K. Shao, W. Sun, X. Yan, X. Peng, NIR light-driving barrier-free group rotation in nanoparticles with an 88.3% photothermal conversion efficiency for photothermal therapy, Adv. Mater. 32 (11) (2020) 1907855, https://doi.org/10.1002/adma.201907855.

[32] V. García-López, F. Chen, L.G. Nilewski, G. Duret, A. Aliyan, A.B. Kolomeisky, J. T. Robinson, G. Wang, R. Pal, J.M. Tour, Molecular machines open cell membranes, Nature 548 (7669) (2017) 567–572, https://doi.org/10.1038/nature23657.

[33] J. Pecourneau, R. Losantos, A. Delova, Y. Bernhard, S. Parant, M. Mourer, A. Pasc, A. Monari, Biomimetic photo-switches softening model lipid membranes, Langmuir 38 (50) (2022) 15642–15655.

[34] J. Pecourneau, R. Losantos, A. Monari, S. Parant, A. Pasc, M. Mourer, Synthesis and photoswitching properties of bioinspired dissymmetric γ-pyrone, an analogue of cyclocurcumin, J. Org. Chem. 86 (12) (2021) 8112–8126, https://doi.org/10.1021/acs.joc.1c00598.

[35] R. Losantos, J. Pecourneau, M. Mourer, S. Parant, A. Pasc, A. Monari, Trans-Cis photoisomerization of a biomimetic cyclocurcumin analogue rationalized by molecular modelling, Phys. Chem. Chem. Phys. 23 (22) (2021) 12842–12849, https://doi.org/10.1039/D1CP01224J.

[36] R. Losantos, A. Pasc, A. Monari, Don't help them to bury the light. The interplay between intersystem crossing and hydrogen transfer in photoexcited curcumin revealed by surface-hopping dynamics, Phys. Chem. Chem. Phys. 23 (2021) 24757–24764.

[37] A. Delova, R. Losantos, J. Pecourneau, Y. Bernhard, M. Mourer, A. Pasc, A. Monari, Phase transitions in lipid bilayers by biomimetic photoswitches based on cyclocurcumin, J. Chem. Inf. Model. 63 (1) (2023) 299–307.

[38] *Antibacterial Mechanism of Curcumin: A Review - Zheng - 2020 - Chemistry & Biodiversity - Wiley Online Library*. https://onlinelibrary-wiley-com.bases-doc.univ-lorraine.fr/doi/10.1002/cbdv.202000171 (accessed 2022-10-25).

[39] A. Adamczak, M. Ożarowski, T.M. Karpiński, Curcumin, a natural antimicrobial agent with strain-specific activity, Pharmaceuticals (Basel) 13 (7) (2020) 153, https://doi.org/10.3390/ph13070153.

[40] R. Adhikary, C.A. Barnes, R.L. Trampel, S.J. Wallace, T.W. Kee, J.W. Petrich, Photoinduced *trans* -to- *cis* isomerization of cyclocurcumin, J. Phys. Chem. B 115 (36) (2011) 10707–10714, https://doi.org/10.1021/jp200080s.

[41] G. Angelini, A. Gansmüller, J. Pécourneau, C. Gasbarri, An insight into cyclocurcumin cis-trans isomerization: kinetics in solution and in the presence of silver nanoparticles, J. Mol. Liq. 333 (2021), 116000, https://doi.org/10.1016/j.molliq.2021.116000.

[42] R.L. Martin, Natural transition orbitals, J. Chem. Phys. 118 (11) (2003) 4775–4777, https://doi.org/10.1063/1.1558471.

[43] X. Zhao, J. Luo, S. Yang, K. Han, New insight into the photoprotection mechanism of plant sunscreens: adiabatic relaxation competing with nonadiabatic relaxation in the cis → trans photoisomerization of methyl sinapate, J. Phys. Chem. Lett. 10 (15) (2019) 4197–4202, https://doi.org/10.1021/acs.jpclett.9b01651.

[44] M. Mlakić, L. Mandić, N. Basarić, B. Mihaljević, F. Pavošević, I. Škorić, Substituents affect the mechanism of photochemical E-Z isomerization of diarylethene triazoles via adiabatic singlet excited state pathway or via triplet excited state, J. Photochem. Photobiol. A Chem. 422 (2022), 113567, https://doi.org/10.1016/j.jphotochem.2021.113567.

[45] E.N. Ushakov, T.P. Martyanov, A.I. Vedernikov, A.A. Efremova, A.A. Moiseeva, L. G. Kuz'mina, S.N. Dmitrieva, J.A.K. Howard, S.P. Gromov, Highly stable supramolecular donor-acceptor complexes involving a bis(18-crown-6)azobenzene as weak donor: structure-property relationships, ACS Omega 5 (40) (2020) 25993–26004.

[46] P. Lentes, E. Stadler, F. Röhricht, A. Brahms, J. Gröbner, F.D. Sönnichsen, G. Gescheidt, R. Herges, Nitrogen bridged diazocines: photochromes switching within the near-infrared region with high quantum yields in organic solvents and in water, J. Am. Chem. Soc. 141 (34) (2019) 13592–13600, https://doi.org/10.1021/jacs.9b06104.

[47] L. Casimiro, S. Maisonneuve, P. Retailleau, S. Silvi, J. Xie, R. Métivier, Photophysical properties of 4-dicyanomethylene-2-methyl-6-(*p* -dimethylamino-styryl)-4 *H*-pyran revisited: fluorescence versus photoisomerization, Chem. Eur. J. 26 (63) (2020) 14341–14350, https://doi.org/10.1002/chem.202002828.

[48] M. Marazzi, A. Francés-Monerris, M. Mourer, A. Pasc, A. Monari, *Trans* -to- *Cis* photoisomerization of cyclocurcumin in different environments rationalized by computational photochemistry, Phys. Chem. Chem. Phys. 22 (8) (2020) 4749–4757, https://doi.org/10.1039/C9CP06565B.

[49] G. Valdomir, J. Padrón, J. Padrón, V. Martín, D. Davyt, Oxazole/thiazole and triazole hybrids based on α-amino acids, Synthesis 46 (18) (2014) 2451–2462, https://doi.org/10.1055/s-0033-1339139.

[50] T. Tahtouh, J.M. Elkins, P. Filippakopoulos, M. Soundararajan, G. Burgy, E. Durieu, C. Cochet, R.S. Schmid, D.C. Lo, F. Delhommel, A.E. Oberholzer, L.H. Pearl, F. Carreaux, J.-P. Bazureau, S. Knapp, L. Meijer, Selectivity, cocrystal structures, and neuroprotective properties of leucettines, a family of protein kinase inhibitors derived from the marine sponge alkaloid leucettamine B, J. Med. Chem. 55 (21) (2012) 9312–9330, https://doi.org/10.1021/jm301034u.

[51] R. Forschner, J. Knelles, K. Bader, C. Müller, W. Frey, A. Köhn, Y. Molard, F. Giesselmann, S. Laschat, Flavylium salts: a blooming core for bioinspired ionic liquid crystals, Chem. Eur. J. 25 (56) (2019) 12966–12980, https://doi.org/10.1002/chem.201901975.

[52] A. Sutter, M. Elhabiri, G. Ulrich, Fluorescent PH-responsive probes based on water-soluble boron-dipyrromethene (BODIPY) derivatives, Featuring long-wavelength emission, *Chem. Eur. J.* 24 (43) (2018) 11119–11130, https://doi.org/10.1002/chem.201801540.

[53] K. Andersson, P.A. Malmqvist, B.O. Roos, A.J. Sadlej, K. Wolinski, Second-order perturbation theory with a CASSCF reference function, J. Phys. Chem. 94 (14) (1990) 5483–5488, https://doi.org/10.1021/j100377a012.

[54] K. Andersson, P. Malmqvist, B.O. Roos, Second-order perturbation theory with a complete active space self-consistent field reference function, J. Chem. Phys. 96 (2) (1992) 1218–1226, https://doi.org/10.1063/1.462209.

[55] A.D. Becke, Density-functional Thermochemistry. III The role of exact exchange, J. Chem. Phys. 98 (7) (1993) 5648–5652, https://doi.org/10.1063/1.464913.

[56] T. Yanai, D.P. Tew, N.C. Handy, A new hybrid exchange-correlation functional using the coulomb-attenuating method (CAM-B3LYP), Chem. Phys. Lett. 393 (1–3) (2004) 51–57, https://doi.org/10.1016/j.cplett.2004.06.011.

[57] Losantos, R.; Pecourneau, J.; Mourer, M.; Parant, S.; Pasc, A.; Monari, A. Trans-Cis Photoisomerization of Biomimetic Cyclocurcumin Analogous Rationalized by Molecular Modelling. **2021**. https://doi.org/10.26434/chemrxiv.14248550.v1.

[58] W.J. Hehre, R. Ditchfield, J.A. Pople, Self—consistent molecular orbital methods. XII. further extensions of Gaussian—type basis sets for use in molecular orbital studies of organic molecules, J. Chem. Phys. 56 (5) (1972) 2257–2261, https://doi.org/10.1063/1.1677527.

[59] F. Aquilante, J. Autschbach, R.K. Carlson, L.F. Chibotaru, M.G. Delcey, L. De Vico, I. Fdez. Galván, N. Ferré, L.M. Frutos, L. Gagliardi, M. Garavelli, A. Giussani, C. E. Hoyer, G. Li Manni, H. Lischka, D. Ma, P.Å. Malmqvist, T. Müller, A. Nenov, M. Olivucci, T.B. Pedersen, D. Peng, F. Plasser, B. Pritchard, M. Reiher, I. Rivalta, I. Schapiro, J. Segarra-Martí, M. Stenrup, D.G. Truhlar, L. Ungur, A. Valentini, S. Vancoillie, V. Veryazov, V.P. Vysotskiy, O. Weingart, F. Zapata, R. Lindh, Molcas

8: new capabilities for multiconfigurational quantum chemical calculations across the periodic table, J. Comput. Chem. 37 (5) (2016) 506–541, https://doi.org/10.1002/jcc.24221.

[60] I. Fdez. Galván, M. Vacher, A. Alavi, C. Angeli, F. Aquilante, J. Autschbach, J. J. Bao, S.I. Bokarev, N.A. Bogdanov, R.K. Carlson, L.F. Chibotaru, J. Creutzberg, N. Dattani, M.G. Delcey, S.S. Dong, A. Dreuw, L. Freitag, L.M. Frutos, L. Gagliardi, F. Gendron, A. Giussani, L. González, G. Grell, M. Guo, C.E. Hoyer, M. Johansson, S. Keller, S. Knecht, G. Kovačević, E. Källman, G. Li Manni, M. Lundberg, Y. Ma, S. Mai, J.P. Malhado, P.Å. Malmqvist, P. Marquetand, S.A. Mewes, J. Norell, M. Olivucci, M. Oppel, Q.M. Phung, K. Pierloot, F. Plasser, M. Reiher, A.M. Sand, I. Schapiro, P. Sharma, C.J. Stein, L.K. Sørensen, D.G. Truhlar, M. Ugandi, L. Ungur, A. Valentini, S. Vancoillie, V. Veryazov, O. Weser, T.A. Wesołowski, P.-O. Widmark, S. Wouters, A. Zech, J.P. Zobel, R. Lindh, OpenMolcas: from source code to insight, J. Chem. Theory Comput. 15 (11) (2019) 5925–5964.

[61] Frisch, M. J.; Trucks, G. W.; Schlegel, H. B. **2016**, *Gaussian, Inc*.

[62] L. Čechová, J. Kind, M. Dračínský, J. Filo, Z. Janeba, C.M. Thiele, M. Cigáň, E. Procházková, Photoswitching behavior of 5-phenylazopyrimidines. In situ irradiation NMR and optical spectroscopy combined with theoretical methods, J. Org. Chem. 83 (11) (2018) 5986–5998, https://doi.org/10.1021/acs.joc.8b00569.

[63] Y. Ji, D.A. DiRocco, J. Kind, C.M. Thiele, R.M. Gschwind, M. Reibarkh, LED-illuminated NMR spectroscopy: A practical tool for mechanistic studies of photochemical reactions, ChemPhotoChem 3 (10) (2019) 984–992, https://doi.org/10.1002/cptc.201900109.

[64] E. Cortelazzo-Polisini, M. Boisbrun, A.H. Gansmüller, C. Comoy, Photoisomerization of arylidene heterocycles: toward the formation of fused heterocyclic quinolines, J. Org. Chem. 87 (15) (2022) 9699–9713, https://doi.org/10.1021/acs.joc.2c00748.

[65] C. Feldmeier, H. Bartling, E. Riedle, R.M. Gschwind, LED Based NMR illumination device for mechanistic studies on photochemical reactions – versatile and simple, yet surprisingly powerful, J. Magn. Reson. 232 (2013) 39–44, https://doi.org/10.1016/j.jmr.2013.04.011.

[66] X. Liu, B. Li, F. Fu, K. Xu, R. Zou, Q. Wang, B. Zhang, Z. Chen, J. Hu, Facile synthesis of biocompatible cysteine-coated CuS nanoparticles with high photothermal conversion efficiency for cancer therapy, Dalton Trans. 43 (30) (2014) 11709, https://doi.org/10.1039/C4DT00424H.

[67] N. Ma, M.-K. Zhang, X.-S. Wang, L. Zhang, J. Feng, X.-Z. Zhang, NIR light-triggered degradable $MoTe_2$ nanosheets for combined photothermal and chemotherapy of cancer, Adv. Funct. Mater. 28 (31) (2018) 1801139, https://doi.org/10.1002/adfm.201801139.